CHALMERS

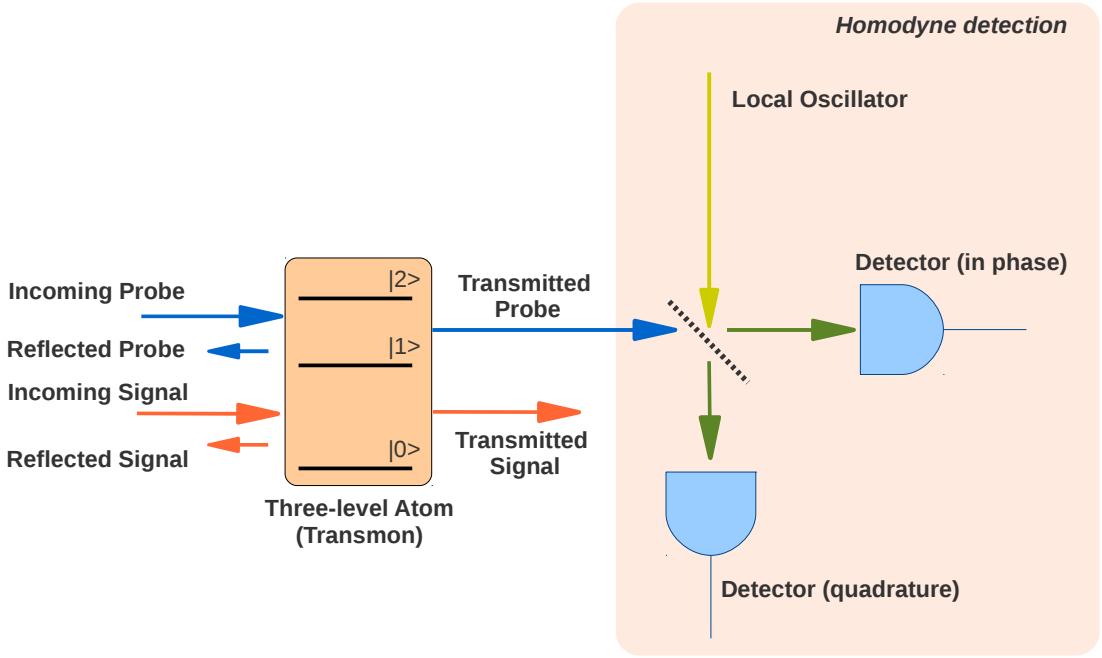

Quantum non-demolition detection of propagating microwave photons

Thesis for Erasmus Mundus Master of Science in Nanoscience and Nanotechnology

Sankar Raman Sathyamoorthy

Department of Microtechnology and Nanoscience-MC2
Chalmers University of Technology
Göteborg, Sweden 2012

Education and Culture DG
ERASMUS MUNDUS

KATHOLIEKE UNIVERSITEIT LEUVEN

Thesis for the degree of Erasmus Mundus Master of Science in Nanoscience and Nanotechnology

Quantum non-demolition detection of propagating microwave photons

Sankar Raman Sathyamoorthy

Promoter & Supervisor: Prof. Göran Johansson, Chalmers
Co-promoter: Prof. Mark Huyse, K.U.Leuven

Department of Microtechnology and Nanoscience-MC2
Chalmers University of Technology
Göteborg, Sweden 2012

This master thesis is conducted in the framework of the Erasmus Mundus Master programme for Nanoscience and Nanotechnology.

Quantum non-demolition detection of propagating microwave photons
Sankar Raman Sathyamoorthy

Applied Quantum Physics Laboratory
Department of Microtechnology and Nanoscience-MC2
Chalmers University of Technology
SE-412 96 Göteborg, Sweden
Telephone: +46 31-772 1000

Cover: Schematic representation of a transmon interacting with two coherent input fields, signal and probe. The homodyne detection is used to measure the phase change in the probe due to the presence of signal.

Chalmers Reproservice
Göteborg, Sweden 2012

Quantum non-demolition detection of propagating microwave photons

Sankar Raman Sathyamoorthy
Department of Microtechnology and Nanoscience-MC2
Chalmers University of Technology, 2012

Abstract

Typical photon counters involve absorption of photons to generate electric signals, thus basically destroying the information carried by the photon. This is all the more disastrous if the photon is used as a quantum information carrier, such as a part of an entangled pair. Quantum non-demolition (QND) measurements are designed to overcome this limitation. Such a non-destructive photon detection would play a key role in quantum networks where photons can be used as "flying" qubits.

In this thesis, using circuit QED we investigate if QND detection of a propagating microwave photon is possible. The system considered consists of a three level artificial atom (transmon) interacting with signal and probe fields. The fields are in the microwave regime with their frequencies on par with the energy levels of the transmon. The interaction of these two fields with the artificial atom, imparts a phase change on the probe field via the cross-Kerr effect. By measuring this phase change, we indirectly infer the presence of the signal.

In this thesis, we investigate if it is possible to achieve a single photon detection, at first using a single transmon and then using multiple transmons. We find that, while single photon detection is not possible with a single transmon, it is indeed possible with multiple transmons under certain conditions. We also find that with multiple transmons, we can have a large phase change in the probe, which might be desirable in other applications.

Keywords: Circuit QED, microwave, QND, photon detection, transmon .

Acknowledgements

This thesis would not have been possible without the help and support of many people. First of all, I would like to thank my supervisor Prof. Göran Johansson, for introducing me to this field and giving me a very interesting project to work on. I greatly appreciate all the time that he took for providing frequent feedbacks and for clarifying my doubts starting from the very basic.

I would also like to thank the other professors, post-docs, Ph.D. and master students in AQP for welcoming me and making me feel as a part of the team. I did enjoy the discussions we had over the weekly meetings. Special thanks goes to Anton Frisk Kockum, for taking the time out to derive the master equations for the multiple transmons, to cross-check the simulations and for filling some of the gaps in my knowledge.

I would also like to thank the Erasmus Mundus Board for providing me the opportunity for pursuing this wonderful masters program. It has been a fun ride for the past two years. Special thanks goes to our EMM-Coordinator Prof. Guido Groeseneken, for all the help he has been providing. I would also like to thank Prof. Mark Huyse for taking up the role of co-promoter for this project.

Lastly, I would like to thank my parents back in India, as well as friends here and back home for all their support.

Sankar Raman Sathyamoorthy,
Göteborg
1/6/12

Contents

1

Introduction and Motivation

The science of light runs like a thread throughout the history of physics. Many of the fields of physics such as wave theory, relativity and quantum electrodynamics have their origins in the need to understand light and its interaction with matter. This thesis involves light-matter interaction at the fundamental level.

In this chapter, we introduce the field of study and motivate the work done. We briefly describe the design and working of the superconducting artificial atoms, in particular motivate why we chose the transmon. Finally, we introduce the concept of Quantum non-demolition measurement.

1.1 Quantum Electrodynamics

Quantum electrodynamics(QED) describes the interaction between light and matter and has been considered as one of the most successful theories of the 20th century. Although the theory is more than half a century old, in the past couple of decades it has been possible to make experiments and observe light-matter in-

teraction at the quantum level in the lab rather easily due to the advancements in technology.

The simplest interesting system in this area is that of a single photon interacting with a single atom. In such experiments, photons are usually confined in a cavity to increase the interaction or coupling between the matter(atom) and light(photon), as the interaction strength between the two is weak in vacuum. In the simplest of cases, the cavity consists of two parallel mirrors and the resulting electromagnetic wave inside the cavity is a standing wave with its nodes on the two mirrors. The atom is then placed in the middle of the cavity and the system is let to evolve (See Fig.1.1). This approach is known as cavity QED.

In recent years, the field of circuit QED has also been growing rapidly [2, 3], rivalling the results obtained with traditional set-ups involving lasers and real atoms. In this case, the photons are microwave photons transmitted via a transmission line and the atoms are artificial ones created using superconducting circuits (See Fig.1.2). It was shown that strong coupling between light and matter is possible in these systems [4], opening up a huge interest in the area culminating in many

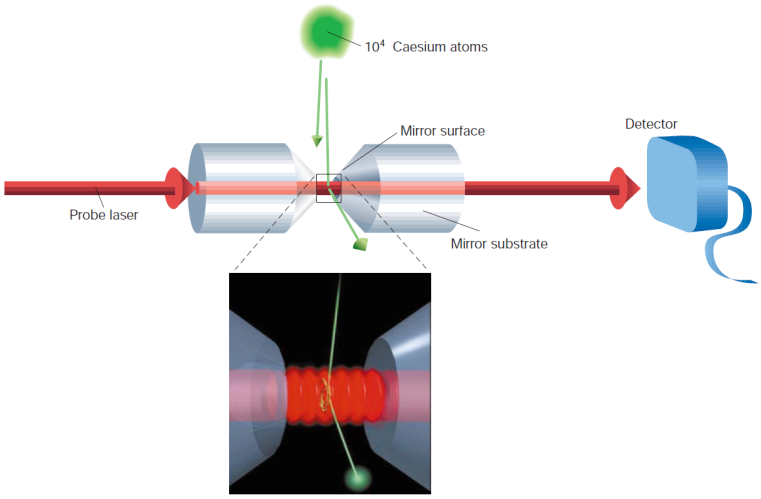

Figure 1.1: Schematic set-up for Cavity QED showing the interaction of Caesium atoms with laser in a cavity. Figure from [1].

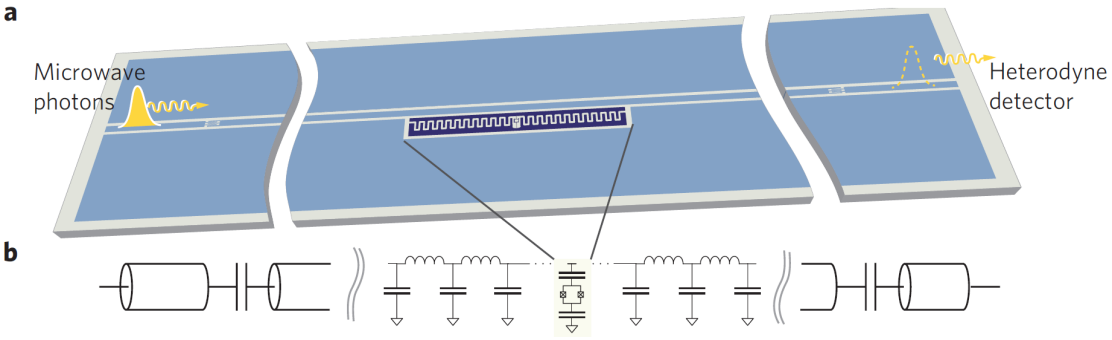

Figure 1.2: Schematic set-up for Circuit QED representing the interaction of microwave photons with artificial atoms. Also shown is the equivalent circuit diagram. Figure from [11].

fundamental experiments [5–10].

Circuit QED has several advantages over traditional systems with optical photons and real atoms. Some of these are listed below

- Can be created on chip using standard nano-fabrication techniques
- Made of solid state systems with tunable parameters
- No alignment problems of light source with the atom, as the photons are guided in the circuits.

There is also a disadvantage as we need to go down to very low temperature for using the superconducting circuits in order to have better coherence time.

Within this area of circuit QED, there is a further interest in working on propagating photons instead of first confining them in a cavity. In this thesis, we investigate if indeed we can detect a photon non-destructively while it is propagating.

1.2 Quantum computers and networks

In his now seminal talk of 1982 [12], R.P.Feynman proposed using quantum computers for simulation of physical phenomena. He argued that such a system would not suffer the limitation of requiring exponential resources to simulate quantum phenomena like a classical computer would require. With the discovery of Shor's algorithm [13] that provides exponential speed-up in prime factorization of large numbers and Grover's algorithm [14] that provides quadratic speed-up in searching an unsorted database, there has been a huge effort in building the first functional quantum computer. Quantum computers have been proposed using various physical systems such as NMR, trapped ions and optical photons in cavity [15]. One of the promising area of implementation is in superconducting circuits [2, 3].

Consider a quantum computer as part of a network. While the processing in the computers can be done using systems mentioned above (called matter qubits), the communication between the nodes would be best done via photons carrying the quantum information (also known as flying qubits).Thus, to have a fully functional superconducting quantum computer as part of a network, we must first design and develop few important devices such as a single photon generator(Fock state generator), a photon router, photon detector/counter. A photon router in superconducting circuits has been shown recently by the team at Chalmers [16]. Currently there is no single photon detector in the microwave regime as the energy carried by microwave photons is very low compared to optical photons. In this thesis, we analyse if it is possible to achieve single microwave photon detection, especially if a non-destructive detection is possible.

1.3 Artificial atoms

The artificial atoms that we consider here are made of superconducting circuits consisting of Josephson junctions in SQUID formation. A Josephson junction is a

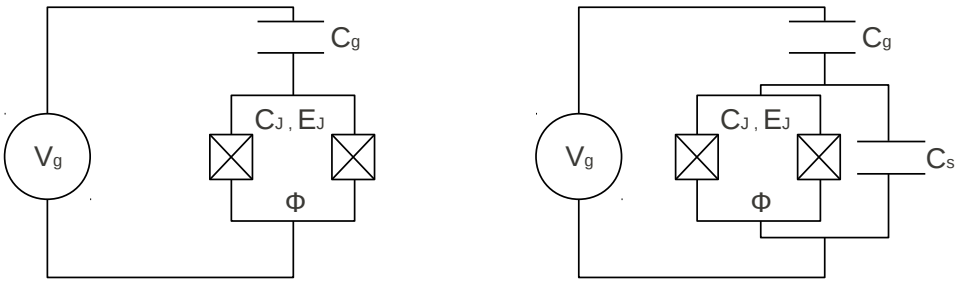

(a) (b)

Figure 1.3: Reduced circuit diagram of (a) Cooper Pair Box (b) Transmon

superconducting tunnel contact consisting of two superconductors separated by a weak link. The Josephson junction is characterized by its capacitance C_J and the Josephson energy E_J. A SQUID (Superconducting Quantum Interference Device) consists of two Josephson junctions connected in parallel to form a loop. In this configuration, the two Josephson junctions act as a single junction with tunable parameters, whose values can be modulated by applying magnetic flux inside the loop.

Various superconducting artificial atoms such as Charge qubits [17, 18], Phase qubits [19, 20] and Flux qubits [21] have been proposed as qubits for use in Quantum Information processing. In this thesis, we will focus on a particular type of superconducting artificial atom called the transmon, although the results can be extended to other operating regimes.

1.3.1 Cooper Pair Box and the Transmon

A Cooper pair box (CPB) can be considered as an island to which the Cooper pairs can tunnel to/from controlled by the gate voltage. The island is connected to the reservoir of Cooper pairs through Josephson junctions in SQUID formation. The simplified circuit diagram of a CPB is shown in Fig.1.3(a).

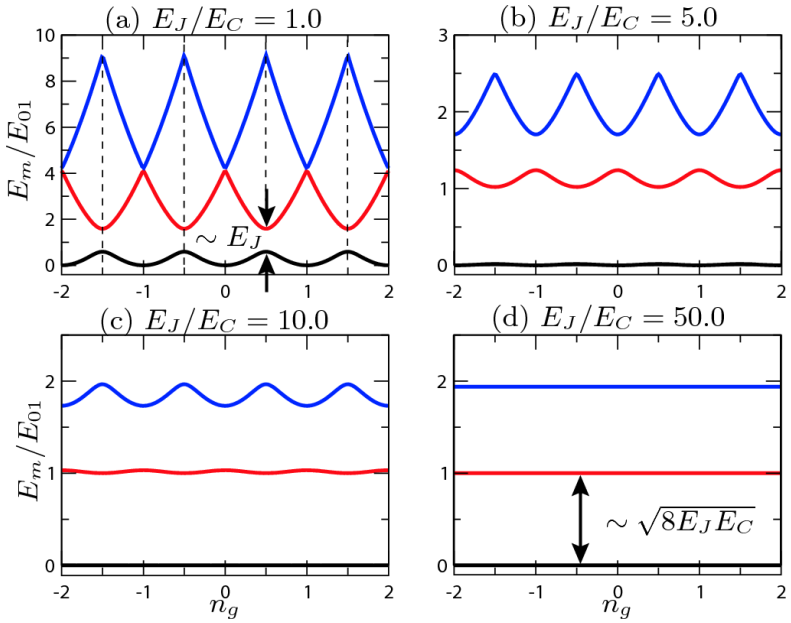

Figure 1.4: Eigen energies for a CPB. Figure from Koch et al [22]. The black arrows in (a) at $n_g = \frac{1}{2}$, shows a sweet spot, where the influence of charge noise is lowest. If the qubit is operated at this point, small fluctuations in n_g doesn't change the energies much as the slope at the point is zero.

An important parameter of operation for the CPB is the ratio E_J/E_C where E_J is the Josephson energy and $E_C = \frac{e^2}{2C_\Sigma}$ is the charging energy, with e being the charge of electron and C_Σ being the total capacitance i.e. the sum of the capacitance of the Josephson junction C_J and gate capacitance C_g . The charge dispersion and the an-harmonicity of the energy spectrum of the qubit as a function of the gate charge $n_g = \frac{C_g V_g}{2e}$ depends on the value of E_J/E_C, as shown in Fig.1.4.

From the figure, we see that with an increase in the value of E_J/E_C, the charge dispersion reduces (good) but also the an-harmonicity reduces (bad). Having flatter bands with respect to the gate charge reduces the effect of charge noise. As we can see from the dispersion figure, if the bands are flatter, small fluctuations in the gate charge doesn't give rise to large changes in the energy. We also need significant an-harmonicity in the energy spectrum to address the individual levels with a particular frequency of input signal. If all of the energy gaps were equidistant, like in the case of an harmonic oscillator, the input signal can couple to any

of the transitions of the artificial atom and we loose the possibility to address the levels we want. Fortunately, we can find a value for E_J/E_C where the charge dispersion is reduced significantly while the an-harmonicity is reduced by relatively lesser amount. This is due the fact that the bands become flatter exponentially faster with increase in the value of E_J/E_C while the an-harmonicity reduces more slowly [23].

Transmons were proposed by Koch et al [22] as an extension of the Cooper pair box (CPB) taking the above detail into account. The Transmon has a large shunt capacitor C_s connected in parallel to the SQUID of a CPB as shown in Fig.1.3 (b). This increases the value of E_J/E_C reducing the charge noise significantly.

Given the reduction of noise and good an-harmonic behaviour of the transmon, they have been implemented in many experiments (For e.g. refer [7, 16, 24–26]).

In this thesis, we use three levels of the transmon (labelled 0,1 and 2) with two coherent fields (called signal and probe) that couple to the two energy transitions (0-1 and 1-2) of the transmon.

1.4 Quantum non-demolition (QND) measurements

Normal photon detectors absorb the photon to generate an excitation (like an electron-hole pair) that is then detected as an electrical signal. This limits the amount of operations that can be performed on a single photon. For example, if we build a quantum computer and use photons as information carriers, we need a way to process them (like storing them or applying gates) after we detect the same. So there is a need to have a detection technique that is non-destructive.

QND measurements were first devised in 1970s to enable detection of gravitational waves [27]. Since then many experiments have been proposed and per-

formed to detect photons non-destructively, both in the optical and microwave regime. (For instance, see references [28–32]). Most of these experiments involve storing the photon in a cavity and probing them with highly excited atoms known as Rydberg atoms. While the cavity helps in increasing the coupling between light and matter, it also brings in certain limitations. For instance, to have a longer lifetime of photons inside the cavity, we require high Q value. But this would make it difficult to transmit the incoming photon into the cavity due to high reflection. As one can imagine, we would like to detect the photon as it gets transmitted instead of first confining it in a cavity. In this thesis, we investigate if quantum non-demolition detection of a propagating microwave photon is possible and thus eliminating the need for a cavity.

1.5 Overview of the thesis

We start in Chapter 2 with an introduction to the Hamiltonian of the system that consists of a transmon coupled to a transmission line with two input coherent drives. We apply the Rotating Wave Approximation(RWA) and transform the Hamiltonian to the rotating frame.

In Chapter 3, we use the Hamiltonian derived in Chapter 2 as part of the master equation. The master equation is an equation for the time evolution of the density matrix of the system coupled to the environment. We solve the master equation to find the steady state solution and from this, we calculate the phase change in the probe field due to the signal field in various limits. In the last part of the chapter, we see if this set-up can be used as a photon detector and the corresponding limitations therein.

In Chapter 4, we extend our system to include more than one transmon and verify how this helps our purpose of photon detection. We investigate different scenarios of connecting the many transmons and check how the behaviour changes.

Finally we conclude in Chapter 5 by highlighting some important results obtained in this thesis and motivate some of the future work that needs to be done.

2

Hamiltonian

In this chapter, we introduce the Hamiltonian of the system under consideration. The system consists of the artificial atom (transmon), coupled to a 1-D coplanar wave-guide through which the microwave photons are transmitted. The wave-guide is a transmission line and can be modelled as series of LC oscillators. Two coherent microwave photons, signal and probe, are sent through the transmission line which then couple to the transmon. The physical set-up considered is shown in Fig.2.1 and the equivalent circuit diagram is shown in Fig.2.3. A micrograph of a system similar to the one considered here is shown in Fig.2.2.

2.1 Hamiltonian in the rotating frame

In this thesis, we consider only 3 levels of the transmon (0,1 and 2) with the input signal field $A_s cos(\omega_s t)$ coupled to the transition 0-1 and the input probe field $A_p cos(\omega_p t)$ coupled to the transition 1-2.

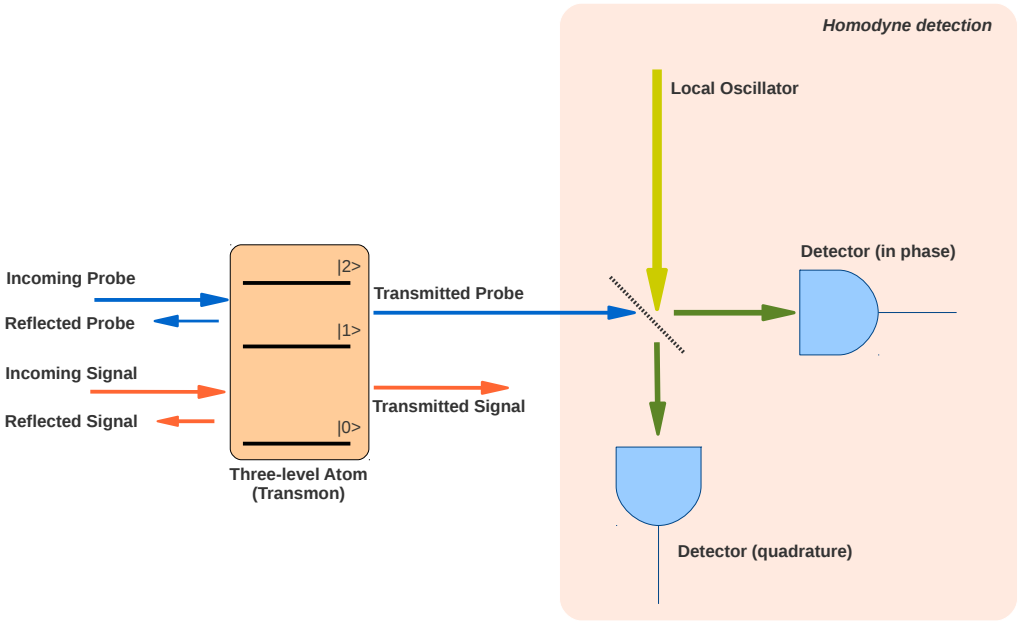

Figure 2.1: Schematic representation of the system considered. The homodyne detection part of the set-up is explained in more detail in the next chapter.

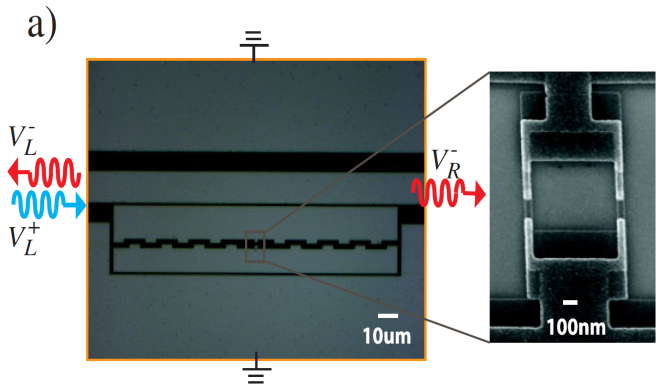

Figure 2.2: A micrograph of transmon embedded in a 1D open transmission line from [16]. This set-up was used to route microwave photons. We use a similar set-up in this thesis for photon detection.

The Hamiltonian of the any 3-level atom in its eigen-basis can be written as

$$H_{tr} = \begin{pmatrix} E_0 & 0 & 0 \\ 0 & E_1 & 0 \\ 0 & 0 & E_2 \end{pmatrix}. \tag{2.1}$$

The Hamiltonian for the input coherent fields are given by

$$H_{drive} = A_s cos(\omega_s t) d_{01}\sigma_{01} + A_p cos(\omega_p t) d_{12}\sigma_{12},$$

where d_{01} and d_{12} are the dipole moments for the 0-1 and 1-2 transitions of the transmon respectively. $A_{s/p}$ and $\omega_{s/p}$ correspond to the amplitude and the frequency of the input coherent fields. In matrix form,

$$H_{drive} = A_s cos(\omega_s t) d_{01} \begin{pmatrix} 0 & 1 & 0 \\ 1 & 0 & 0 \\ 0 & 0 & 0 \end{pmatrix} + A_p cos(\omega_p t) d_{12} \begin{pmatrix} 0 & 0 & 0 \\ 0 & 0 & 1 \\ 0 & 1 & 0 \end{pmatrix}. \tag{2.2}$$

The total Hamiltonian of the system is given by,

$$H_{sys} = H_{tr} + H_{drive}. \tag{2.3}$$

We can simplify the problem by going to a different frame of reference called the interaction picture or the rotating frame. To do this we define the following unitary matrix

$$\mathcal{R} = \begin{pmatrix} e^{i\left(\frac{E_1}{\hbar} - \omega_s\right)t} & 0 & 0 \\ 0 & e^{\frac{iE_1 t}{\hbar}} & 0 \\ 0 & 0 & e^{i\left(\frac{E_1}{\hbar} + \omega_p\right)t} \end{pmatrix}.$$

From the time dependent Schrödinger equation, it can be shown that the Hamil-

tonian in the rotating frame is given by,

$$H_{sys}^{rf} = \mathcal{R} H_{sys} \mathcal{R}^{\dagger} + i\hbar \frac{\partial \mathcal{R}}{\partial t} \mathcal{R}^{\dagger}.$$

Substituting the values from above, we get

$$H_{sys}^{rf} = \begin{pmatrix} \mathrm{E}_0 - \mathrm{E}_1 + \hbar\omega_s & \frac{1}{2}\mathrm{A}_s \left(1 + e^{-2i\omega_s t}\right) d_{01} & 0 \\ \frac{1}{2}\mathrm{A}_s \left(1 + e^{2i\omega_s t}\right) d_{01} & 0 & \frac{1}{2}\mathrm{A}_p \left(1 + e^{-2i\omega_p t}\right) d_{12} \\ 0 & \frac{1}{2}\mathrm{A}_p \left(1 + e^{2i\omega_p t}\right) d_{12} & -\mathrm{E}_1 + \mathrm{E}_2 - \hbar\omega_p \end{pmatrix}, \tag{2.4}$$

where we have used the identity

$$cos\theta = \frac{e^{i\theta} + e^{-i\theta}}{2}.$$

Applying the Rotating Wave Approximation (RWA), we ignore the fast rotating terms containing $2\omega_s$ and $2\omega_p$ as these terms average out to 0 in the time scales relevant to the problem. This approximation is valid as long as the strength of the input fields is not high compared to the energy difference of the levels of the transmon, i.e. RWA is valid as long as $A_s d_{01} < E_1 - E_0$ and $A_p d_{12} < E_2 - E_1$. With RWA, the Hamiltonian in the rotating frame reduces to

$$H_{sys}^{rf} = \begin{pmatrix} \mathrm{E}_0 - \mathrm{E}_1 + \hbar\omega_s & \frac{1}{2}\mathrm{A}_s d_{01} & 0 \\ \frac{1}{2}\mathrm{A}_s d_{01} & 0 & \frac{1}{2}\mathrm{A}_p d_{12} \\ 0 & \frac{1}{2}\mathrm{A}_p d_{12} & -\mathrm{E}_1 + \mathrm{E}_2 - \hbar\omega_p \end{pmatrix}. \tag{2.5}$$

Defining the Rabi frequencies Ω_s and Ω_p of the transitions as

$$\hbar\Omega_s = A_s d_{01} \; ; \; \hbar\Omega_p = A_p d_{12} \tag{2.6}$$

and rewriting the energy differences as

$$E_1 - E_0 = \hbar\omega_{01} \; ; \; E_2 - E_1 = \hbar\omega_{12},$$

we have,

$$H_{sys}^{rf} = \begin{pmatrix} -\hbar\omega_{01} + \hbar\omega_s & \frac{1}{2}\hbar\Omega_s & 0 \\ \frac{1}{2}\hbar\Omega_s & 0 & \frac{1}{2}\hbar\Omega_p \\ 0 & \frac{1}{2}\hbar\Omega_p & \hbar\omega_{12} - \hbar\omega_p \end{pmatrix}.$$

Defining the signal and probe detunings as,

$$\Delta s = \omega_{01} - \omega_s \; ; \; \Delta p = \omega_{12} - \omega_p,$$

we get,

$$H_{sys}^{rf} = \hbar \begin{pmatrix} -\Delta s & \frac{1}{2}\Omega_s & 0 \\ \frac{1}{2}\Omega_s & 0 & \frac{1}{2}\Omega_p \\ 0 & \frac{1}{2}\Omega_p & \Delta p \end{pmatrix},$$

which is the same as

$$H_{sys}^{rf} = \hbar \begin{pmatrix} -\Delta \mathrm{s} & 0 & 0 \\ 0 & 0 & 0 \\ 0 & 0 & \Delta \mathrm{p} \end{pmatrix} + \frac{\hbar\Omega_s}{2} \begin{pmatrix} 0 & 1 & 0 \\ 1 & 0 & 0 \\ 0 & 0 & 0 \end{pmatrix} + \frac{\hbar\Omega_p}{2} \begin{pmatrix} 0 & 0 & 0 \\ 0 & 0 & 1 \\ 0 & 1 & 0 \end{pmatrix}, \quad (2.7)$$

where we have written down the transmon Hamiltonian and the drive Hamiltonians separately similar to eq.(2.3).

2.2 Normalization

The Hamiltonian can be derived from first principles by quantizing the circuit shown in Fig.2.3. A detailed derivation for the case of having a transmon in a

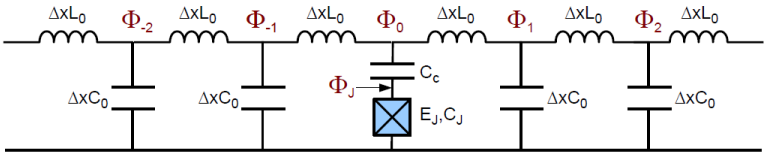

Figure 2.3: Equivalent circuit diagram of a transmon (blue box) coupled to a transmission line. Figure from [33].

cavity is given in [22]. In this thesis, we follow the derivation done in [33] where the system consists of a transmon coupled to an open transmission line as shown in Fig.2.3. We do this to find a suitable normalization for the coherent fields. From this reference, we get the corresponding Hamiltonian in the transmon eigen basis as

$$H_{sys} = \sum_{i=0}^{\infty} \hbar\omega_i |i\rangle\langle i| + \kappa V_{in}(t) \sum_{i,j} |i\rangle\langle j| \langle i|X|j\rangle,$$

where κ is the coupling (in units of charge) between the incoming drive and the transmon and X is the charge operator. Considering only 3 levels with two coherent drives, this would correspond to

$$H_{sys} = \sum_{i=0}^{2} \hbar\omega_i |i\rangle\langle i| + \kappa V_{sig}^{in}(t) \left(|0\rangle\langle 1|\langle 0|X|1\rangle + h.c.\right) + \kappa V_{prb}^{in}(t) \left(|1\rangle\langle 2|\langle 1|X|2\rangle + h.c.\right),$$

as the terms containing $\langle 0|X|2\rangle$ and $\langle 2|X|0\rangle$ are negligible for the transmon. The last two terms in the above Hamiltonian are the drive terms. The coherent voltage drives can be written as,

$$V_{sig/prb}^{in}(t) = V_{sig/prb}^{in}(0) \cos\omega_{s/p} t = V_{sig/prb}^{in}(0) \left(\frac{e^{iw_{s/p}t} + e^{-iw_{s/p}t}}{2} \right).$$

Consider only the second part of the Hamiltonian above, which is for the input signal field interacting with the 0-1 transition of the transmon. Using the Rotating Wave Approximation, and assuming $\langle 0|X|1\rangle$ to be real and positive, this term reduces to

$$H_{sig} = \frac{\kappa V_{sig}^{in}(0)}{2} \langle 0|X|1\rangle \left(|0\rangle\langle 1| + |1\rangle\langle 0|\right) = \frac{\kappa V_{sig}^{in}(0)}{2} \langle 0|X|1\rangle \sigma_{01}.$$

Comparing with corresponding term in eq.(2.7), we see that,

$$\hbar\Omega_s = \kappa V_{sig}^{in}(0)\langle 0|X|1\rangle. \tag{2.8}$$

Similarly, we have

$$\hbar\Omega_p = \kappa V_{prb}^{in}(0)\langle 1|X|2\rangle. \tag{2.9}$$

We normalize the drive with number of photons in the drive per interaction time, which is given by,

$$N = \frac{\text{Power of the drive}}{\text{Energy of each photon}} \times \text{Interaction time.}$$

That is

$$N_{sig}^{in} = \frac{V_{sig}^{in}(0)^2}{2Z_0}\frac{1}{\hbar\omega_s}\frac{1}{\Gamma_s},$$

and

$$N_{prb}^{in} = \frac{V_{prb}^{in}(0)^2}{2Z_0}\frac{1}{\hbar\omega_p}\frac{1}{\Gamma_p},$$

where $Z_0 = \sqrt{\frac{L_0}{C_0}}$ is the impedance of the transmission line. The interaction times are defined as the inverse of the relaxation rates ($\Gamma_{s/p}$) of the transitions. The relaxation rates in the transmon regime are given as

$$\Gamma_{ij} = \kappa^2 \frac{Z_0}{\hbar}\omega_{ij}\left(1 + n_{\omega_{ij}}\right)|\langle i|X|j\rangle|^2,$$

where $n_{\omega_{ij}}$ is the number of photons with frequency ω_{ij}, representing the thermal noise. Taking the temperature to be 0 K, we have $n_{\omega_{ij}} = 0$. This gives the relaxation rates for the two transitions as

$$\Gamma_s = \Gamma_{01} = \kappa^2 \frac{Z_0}{\hbar}\omega_s|\langle 0|X|1\rangle|^2,$$

and

$$\Gamma_p = \Gamma_{12} = \kappa^2 \frac{Z_0}{\hbar}\omega_p|\langle 1|X|2\rangle|^2.$$

Using the above definitions and substituting them in eqs.(2.8) and (2.9) we get,

$$\Omega_s = \sqrt{2}\Gamma_s\sqrt{N_{sig}^{in}}, \tag{2.10}$$

and

$$\Omega_p = \sqrt{2}\Gamma_p\sqrt{N_{prb}^{in}}. \tag{2.11}$$

Thus the Hamiltonian in the Eq. (2.7) can be rewritten with this normalization as,

$$H_{sys}^{rf} = \hbar \begin{pmatrix} -\Delta\mathrm{s} & 0 & 0 \\ 0 & 0 & 0 \\ 0 & 0 & \Delta\mathrm{p} \end{pmatrix} + \hbar\frac{\Gamma_s\sqrt{N_{sig}^{in}}}{\sqrt{2}} \begin{pmatrix} 0 & 1 & 0 \\ 1 & 0 & 0 \\ 0 & 0 & 0 \end{pmatrix} + \hbar\frac{\Gamma_p\sqrt{N_{prb}^{in}}}{\sqrt{2}} \begin{pmatrix} 0 & 0 & 0 \\ 0 & 0 & 1 \\ 0 & 1 & 0 \end{pmatrix}.$$

To simplify further, we use the convention of setting $\hbar \to 1$. This gives us,

$$H_{sys}^{rf} = \begin{pmatrix} -\Delta\mathrm{s} & 0 & 0 \\ 0 & 0 & 0 \\ 0 & 0 & \Delta\mathrm{p} \end{pmatrix} + \Gamma_s\sqrt{\frac{N_{sig}^{in}}{2}} \begin{pmatrix} 0 & 1 & 0 \\ 1 & 0 & 0 \\ 0 & 0 & 0 \end{pmatrix} + \Gamma_p\sqrt{\frac{N_{prb}^{in}}{2}} \begin{pmatrix} 0 & 0 & 0 \\ 0 & 0 & 1 \\ 0 & 1 & 0 \end{pmatrix}. \tag{2.12}$$

This is the Hamiltonian that will be used as part of the master equations in the forthcoming chapters.

3

Single Transmon

In this chapter, we investigate the possibility of performing QND detection of a signal photon using a probe photon and a single transmon. We do this by solving the master equation to find the steady state solutions. The solutions are analysed at different limits to gain insights and to find the optimal values for photon detection. The physical set-up considered is the same as the one described in previous chapter (See Fig.2.1).

3.1 Cross-Kerr interaction

The type of interaction that is considered here is called the cross-Kerr interaction. The presence of the signal drive manifests itself as a phase change in the probe field. By measuring the phase change in the probe we determine if there was a signal or not. Fig.3.1 shows schematically how this works, where the top part of the diagram shows the interaction between the fields and the transmon, while the bottom part shows the amplitude and phase of the transmitted probe photon in an IQ diagram. The IQ diagram is a amplitude-phase diagram where I stands for "In-phase" and

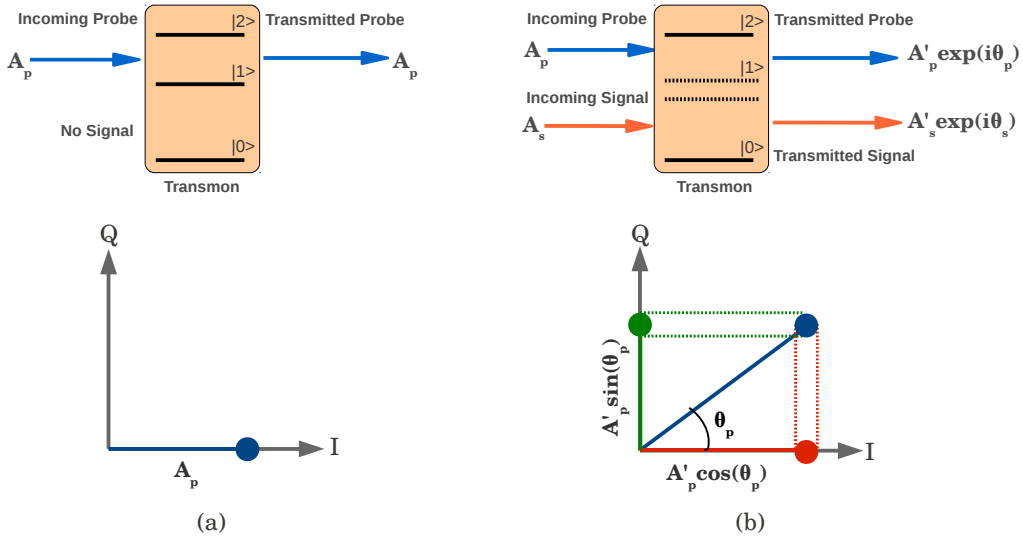

Figure 3.1: Cross-Kerr interaction

Q for "Quadrature". The length of the blue line represents the amplitude of the transmitted probe field while the angle with the I axis gives the phase change in the probe. The uncertainty/noise in the coherent field is represented as a circle at the end of the line whose radius is of the order of $\sqrt{N}$, where N is the mean photon number of the field.

In Fig.3.1(a), we have the situation when there is no signal photon. The atom (transmon) stays in its ground state. The probe photons don't see any excitations in level |1> and hence just pass through without any interaction with the transmon. The amplitude and the phase of the transmitted probe are same as that of the input probe field. As we can see in the IQ diagram, in this case, we don't detect any signal in the Quadrature.

When we have a signal photon, as shown in Fig.3.1(b), the transmon gets excited from the ground level. This results in a splitting of the level |1>, which is of the same order as the amplitude of the input signal A_s. The probe photon now interacts with the transmon due to the presence of the excitations in level |1>, which results in a change in the phase of the probe photon, denoted by the

angle θ_p in the IQ diagram. Ideally, the amplitude of the probe remains the same as the cross-Kerr interaction only introduces a phase shift. But in our case, we have losses due to spontaneous emission (incoherent losses) and due to reflection. Hence, the amplitude of the probe reduces to A'_p. The IQ diagram in Fig.3.1(b) shows the above facts. As shown in the figure, we can project this transmitted probe field on to the I and Q axis, where the cosine and sine components can be measured to read out the amplitude and phase of the transmitted probe.

3.2 Homodyne detection

Standard photon detectors measure the intensity of the light falling on them, which is independent of the phase of the photon. To measure the phase change in the probe we use Homodyne detection. In this, the transmitted probe is mixed with a strong field from a local oscillator. The phase of the local oscillator field is known and can be tuned according to our needs. The mixed signal is then passed through a beam splitter and the strength of the field in phase and in quadrature is measured. This is shown schematically in Fig.2.1. As explained in the previous section, the in-phase measurement gives the cosine component and quadrature measurement gives the sine component of the transmitted probe. Thus from these measurements, we can calculate the amplitude and phase of the transmitted probe field.

3.3 Master equation

Following the derivation of the Hamiltonian in chapter 2, we proceed with the master equation for the system considered in Fig.2.1. The master equation is a time evolution equation of the density matrix of the system coupled to the environment. The master equation can be considered as a more realistic version of the time dependent Schrödinger equation as no system in practice is completely

isolated from the environment. For a more detailed introduction to the master equation, refer [34].

From [34] (5.4.12), the master equation for a system coupled to the environment is given as

$$\dot{\rho} = \frac{i}{\hbar}\left[\rho, H_{sys}\right] + \frac{\gamma}{2}\left(1+\bar{N}\right)\mathcal{D}\left[X\right]\rho + \frac{\gamma}{2}\bar{N}\mathcal{D}\left[X\right]\rho,$$

where

$$\mathcal{D}\left[\hat{c}\right]\rho = \left(2\hat{c}\rho\hat{c}^{\dagger} - \hat{c}\rho\hat{c}^{\dagger} - \hat{c}\rho\hat{c}^{\dagger}\right),$$

and $\bar{N}$ is the number of photons in the environment with the same frequencies as the eigen frequencies of the system. Considering a single transmon with two drives at 0 K (i.e. with $\bar{N} = 0$), we have the master equation (with $\hbar = 1$) as

$$\dot{\rho} = i\left[\rho, H_{sys}\right] + \frac{\gamma_s}{2}\mathcal{D}\left[\sigma_{01}\right]\rho + \frac{\gamma_p}{2}\mathcal{D}\left[\sigma_{12}\right]\rho,$$

where H_{sys} contains the Hamiltonian of the transmon and the two drives. In the rotating frame, we have

$$\dot{\rho}^{rf} = i\left[\rho^{rf}, H^{rf}_{sys}\right] + \frac{\gamma_s}{2}\mathcal{D}\left[\sigma^{-}_{01}\right]\rho^{rf} + \frac{\gamma_p}{2}\mathcal{D}\left[\sigma^{-}_{12}\right]\rho^{rf}.$$

The σ^{-} operators in the above equation are given by,

$$\sigma^{-}_{01} = \begin{pmatrix} 0 & 1 & 0 \\ 0 & 0 & 0 \\ 0 & 0 & 0 \end{pmatrix}; \sigma^{-}_{12} = \begin{pmatrix} 0 & 0 & 0 \\ 0 & 0 & 1 \\ 0 & 0 & 0 \end{pmatrix}, \tag{3.1}$$

and H^{rf}_{sys} is the same as in eq.(2.12)

3.3.1 Solutions of the Master equation

The above master equation is solved to find the steady state density matrix ρ^{ss} of the system in the rotating frame. Considering only coherent output fields, we average out the fields radiated by the transmon. In units of frequency, this is given as

$$\Omega_s^{rad} = i\Gamma_s < \sigma_{01}^- >;\ \Omega_p^{rad} = i\Gamma_p < \sigma_{12}^- > .$$

The expectation value of any operator $\mathcal{O}$ can be calculated as $tr(\rho\mathcal{O})$. Thus we have,

$$< \sigma_{01}^- >= tr(\rho^{ss}\sigma_{01}^-) = tr\left[\begin{pmatrix} \rho_{00}^{ss} & \rho_{01}^{ss} & \rho_{02}^{ss} \\ \rho_{10}^{ss} & \rho_{11}^{ss} & \rho_{12}^{ss} \\ \rho_{20}^{ss} & \rho_{21}^{ss} & \rho_{22}^{ss} \end{pmatrix} \begin{pmatrix} 0 & 1 & 0 \\ 0 & 0 & 0 \\ 0 & 0 & 0 \end{pmatrix}\right] = \rho_{10}^{ss}.$$

Similarly, we have

$$< \sigma_{12}^- >= \rho_{21}^{ss}.$$

Thus, the average coherent field radiated from the transmon is given by,

$$\Omega_s^{\mathrm{rad}} = i\Gamma_s\rho_{10}^{ss};\ \Omega_p^{\mathrm{rad}} = i\Gamma_p\rho_{21}^{ss}.$$

The total transmitted field is given as the sum of the input field and the field radiated by the transmon

$$\Omega_s^{trans} = \Omega_s + \Omega_s^{rad} = |\Omega_s^{trans}|e^{\mathrm{i}\theta_s},$$

and

$$\Omega_p^{trans} = \Omega_p + \Omega_p^{rad} = |\Omega_p^{trans}|e^{\mathrm{i}\theta_p},$$

where the angles θ_s and θ_p represent the phase change in the transmitted signal and probe respectively. These can be calculated as

$$\theta_{s/p} = \text{ArcTan}\left[\frac{\text{Im}(\Omega_{s/p}^{trans})}{\text{Re}(\Omega_{s/p}^{trans})}\right].$$

The reflected fields are given as

$$\Omega_s^{ref} = -\Omega_s^{rad} \; ; \; \Omega_p^{ref} = -\Omega_p^{rad}.$$

Using the normalization derived in the equations (2.10) and (2.11), we get the number of photons in the transmitted fields per interaction time as

$$N_{sig}^{trans} = \frac{|\Omega_s^{trans}|^2}{2\Gamma_s^2} \; ; \; N_{prb}^{trans} = \frac{|\Omega_p^{trans}|^2}{2\Gamma_p^2},$$

and the number of photons in the reflected fields per interaction time as

$$N_{sig}^{ref} = \frac{|\Omega_s^{ref}|^2}{2\Gamma_s^2} \; ; \; N_{prb}^{ref} = \frac{|\Omega_p^{ref}|^2}{2\Gamma_p^2}.$$

3.4 Phase change in the probe

In this section, we look in more detail the phase change induced in the probe due the presence of signal photons. We do this by solving the problem in different regimes starting from the weak limits as described below.

3.4.1 Weak signal and weak probe limit

We first investigate the phase change in the probe in the weak limits (i.e. with N_{sig}^{in} and $N_{prb}^{in} \ll 1$) as the equations simplify considerably in this regime.

The phase change on the probe due to the presence of the signal photon as

shown above is given by

$$\theta_p = \text{ArcTan}\left[\frac{\text{Im}(\Omega_p^{trans})}{\text{Re}(\Omega_p^{trans})}\right].$$

Solving for Ω_p^{trans} and expanding it to the first order in N_{sig}^{in} we get,

$$\theta_p = \text{ArcTan}\left[\frac{4{\Gamma_p}{\Gamma_s}^2(\Delta\text{p}+\Delta\text{s})N_{sig}^{in}}{2{\Gamma_p}^2{\Gamma_s}^2 N_{sig}^{in} - \left({\Gamma_s}^2+4\Delta\text{s}^2\right)\left({\Gamma_p}^2+4(\Delta\text{p}+\Delta\text{s})^2\right)}\right]. \tag{3.2}$$

The above equation shows that, in this regime the phase change is independent of the strength of the probe field. We find the maximum phase change on the probe signal by differentiating the above equation with respect to Δs and Δp and setting it to 0. This gives the value of Δs and Δp for maximum phase change as

$$\Delta\text{s} = 0; \Delta\text{p} = \pm\frac{\Gamma_p\sqrt{(1-2N_{sig}^{in})}}{2}, \tag{3.3}$$

and the corresponding maximum phase change in the probe is,

$$\theta_p^{max} = \text{ArcTan}\left[\frac{N_{sig}^{in}}{\sqrt{1-2N_{sig}^{in}}}\right] \approx N_{sig}^{in}. \tag{3.4}$$

We see from the above derivations that in the weak limits (i.e. with N_{sig}^{in} and $N_{prb}^{in} \ll 1$), the phase change in the probe is linear with the power of the signal field and is independent of the strength of the probe field.

3.4.2 Weak signal and strong probe limit

As it can be imagined, the signal in a quantum communication device might be weak. But the probe photons are generated at the detector to measure the signal

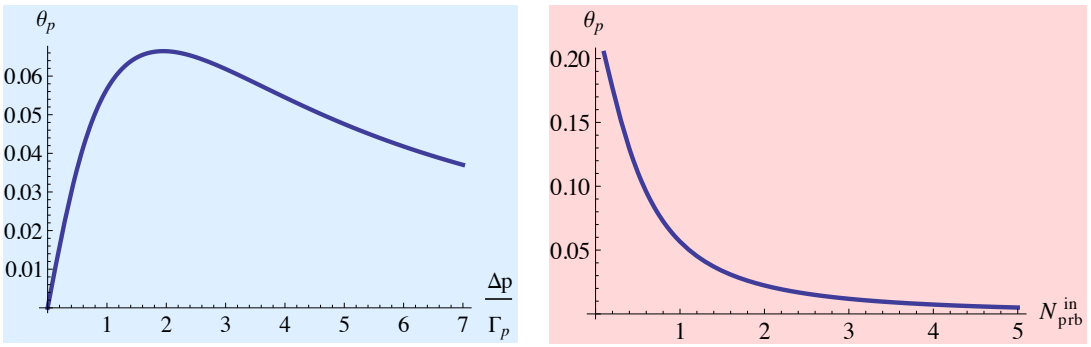

(a) (b)

Figure 3.2: Phase change (in degrees) in a strong probe with a weak signal, calculated as a function of (a) Δp with N^{in}_{prb}=1=200N^{in}_{sig} and (b) N^{in}_{prb} with Δp=Γ_p.

photons. So the probe photons can be created with whatever amplitude we desire. To have fast measurement, we need to have a probe field of significant strength. Hence, we now check for the phase change in the probe when the signal is weak but the probe is stronger.

Parameters and results

As the system involves many variables, in order to gain some intuition about the problem, we fix few of these parameters as described below and check how the phase change in the probe varies with regards to the other parameters. As we see from the above calculations for weak signal and weak probe, the maximum phase change in the probe is achieved when the signal is on resonance i.e. Δs=0. Hence we do the following calculations in the same limit.

The results are shown in Fig.3.2. The signal strength for these results is set by taking N^{in}_{sig}=0.005 which is much less than 1. As we can see from the Fig.3.2(a), the maximum phase occurs when Δp is approximately same as Γ_p. From Fig.3.2(b), we see that the phase change decreases monotonically with increasing probe power. The maximum phase drops to one-fourth of its value when the probe power is increased from N^{in}_{prb}=0.1=20N^{in}_{sig} to N^{in}_{prb}=1=200N^{in}_{sig}. The higher the probe strength

compared to the signal strength, the weaker is the impact of the signal photon on the probe and hence smaller phase change in the probe.

3.4.3 Full Range analysis

Having gained some intuition from the weak limit analysis, we check for the phase change in the probe across the whole range of values applicable. As it can be deduced, the equations derived in this range are complex and analytical solutions are not possible. So we look at how the phase change varies with regards to each of the parameters, by fixing the value for others. The results are shown in figures 3.3 - 3.6. From the figures, we see that the maximum phase change in the probe is obtained when we have a strong signal and a weak probe, with the signal being on resonance (i.e. Δs=0) and with the probe detuning Δp $\approx \Gamma_p$. These values are in-line with our conclusions from the previous sections.

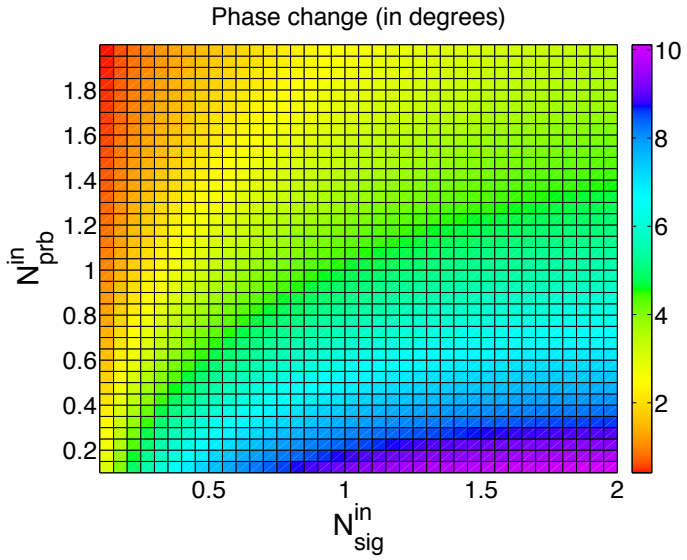

Figure 3.3: Phase change (in degrees) in the probe as a function of number of input photons per interaction time. The value of the other parameters are Δs=0 and Δp=Γ_p=2Γ_s. From the figure, we see that the phase change is maximum when the signal field is strong and the probe field is weak (as expected intuitively).

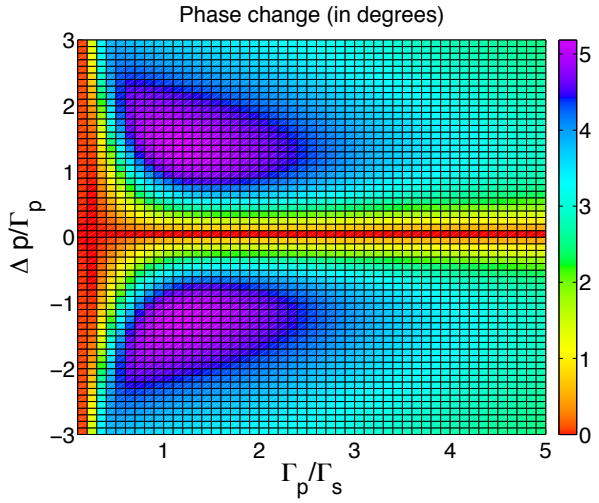

Figure 3.4: Phase change (in degrees) in the probe as a function of probe detuning and relaxation rate. The value of the other parameters are Δs=0, N^{in}_{sig}=1 and N^{in}_{prb}=1. From the figure, we see a symmetric behaviour with the change in sign for Δp. Also we see that when Δp=0, there is no phase change in the probe. (As the signal field splits the level $|1>$, at $\Delta_p = 0$ there is no energy level present for the probe to interact with. Hence there is no phase change in the probe at this value.)

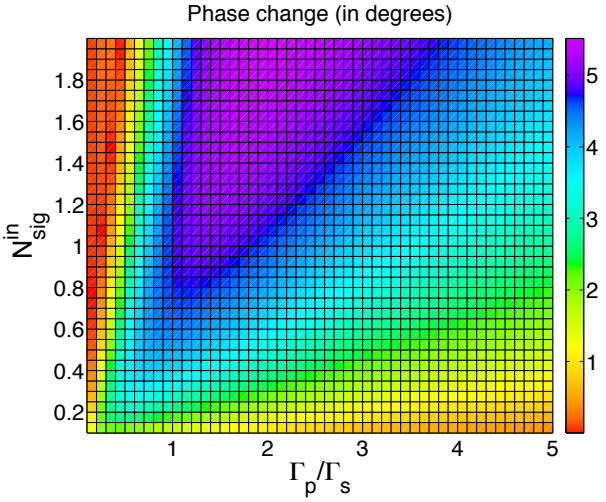

Figure 3.5: Phase change (in degrees) in the probe as a function of N^{in}_{sig} and probe relaxation rate Γ_p. The value of the other parameters are Δs=0, N^{in}_{prb}=1 and Δp=Γ_p. Here we see that at low signal strengths it is better to have $\Gamma_p = \Gamma_s$ but for higher signal strengths it is better to be in the transmon regime i.e. with $\Gamma_p = 2\Gamma_s$.

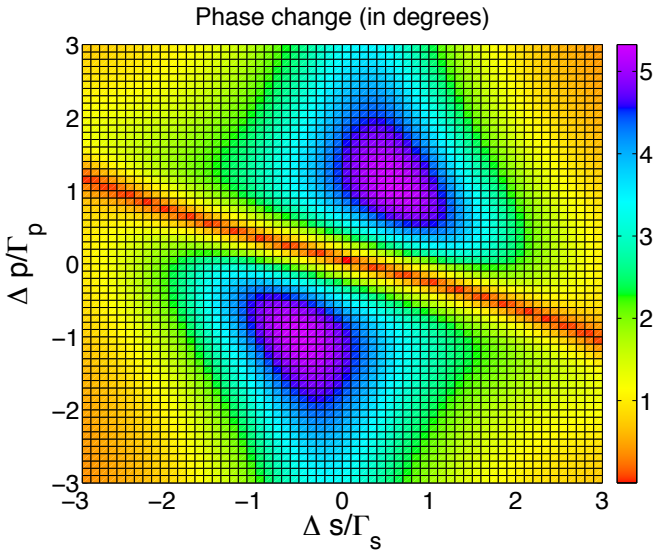

Figure 3.6: Phase change (in degrees) in the probe as a function of probe detuning and signal detuning. The value of the other parameters are N_{sig}^{in}=1, N_{prb}^{in}=1 and Γ_p=2Γ_s. Here again we find that the maximum phase shift is obtained when $\Delta p \approx \Gamma_p$ and $\Delta s \approx 0$ confirming our previous conclusions.

3.5 Photon detection

After analysing the phase change in the probe, we now consider how to use this interaction to detect the signal photons by measuring the probe photons. As explained in the section 3.1, by measuring in the two quadratures for the probe photon and by detecting a change in the probe field, we can indirectly infer the presence of the signal photon. In this section, we formulate few measures to characterize photon detection such as the minimum number of signal photons required to make a detection and check how these values change with different parameters.

3.5.1 Signal-to-noise ratio and minimum number of photons required to detect

Our detection limits are set by noise. In this thesis, we have taken the temperature to be 0 K and hence we don't have any thermal noise in the system. The noise that we consider here comes from the uncertainty relations. For a coherent field, this can be considered as the variance of the pulse around the mean photon number.

To have a good detection, we need the signal-to-noise ratio(SNR) to be greater than 1. Based on this consideration, we derive the minimum number of signal photons required to make a detection using the set-up that we described in section 3.1.

From [35] (6.11.17), we have the signal-to-noise ratio for the Homodyne detection of the probe output as

$$SNR = 4FT\cos^2(\chi - \theta_p),$$

with photon flux, $F = N_{prb}^{trans}\Gamma_p$ where N_{prb}^{trans} is the number of probe photons transmitted from the transmon per interaction time. The axis of measurement is set by $\chi = \theta_L + \pi/2$ where θ_L is the phase of the local oscillator. θ_p is the phase change in the probe and T is the measurement time.

When θ_L=0, we measure the field in the quadrature and when $\theta_L = \pi/2$, we measure in phase. The above formula for SNR works straight-forwardly for θ_L=0 as the quadrature gets a signal only in the presence of the input signal photon as explained in section 3.1.

When $\theta_L = \pi/2$, we are measuring in phase and there are always output probe photons irrespective of the signal. In this case we are interested in the change in amplitude with and without the signal. Without the signal photons, the probe would have just passed through the transmon with no phase change. So for the

measurement in phase, the input field to the Homodyne detector is given by

$$S = \sqrt{N_{prb}^{in}\Gamma_p T}\cos(\chi) - \sqrt{N_{prb}^{trans}\Gamma_p T}\cos(\chi - \theta_p).$$

Thus, we rewrite the above SNR as the following two equations.
For measuring in quadrature:

$$SNR_Q = 4FT_Q\cos^2(\chi - \theta_p) = 4N_{prb}^{trans}\Gamma_p T_Q\cos^2(\chi - \theta_p). \tag{3.5}$$

For measuring in phase:

$$SNR_I = 4[\sqrt{N_{prb}^{in}\Gamma_p T_I}\cos(\chi) - \sqrt{N_{prb}^{trans}\Gamma_p T_I}\cos(\chi - \theta_p)]^2.$$

$$\begin{aligned} \Rightarrow SNR_I &= 4\Gamma_p T_I[N_{prb}^{in}\cos^2(\chi) + N_{prb}^{trans}\cos^2(\chi - \theta_p) \\ &\quad -2\sqrt{N_{prb}^{in}N_{prb}^{trans}}\cos(\chi)\cos(\chi - \theta_p)]. \end{aligned} \tag{3.6}$$

We set SNR=1 in the above equations and calculate the minimum time required to measure, $T_{Q/I}$. During this measurement time, the number of signal photons to pass through the transmon is given by

$$N_{sigQ/I}^{tot} = N_{sig}^{in}\Gamma_s T_{Q/I}, \tag{3.7}$$

where N_{sig}^{in} is the number of input signal photons per interaction time. This gives the minimum number of signal photons required to make a detection. We would like to have the value of $N_{sigQ/I}^{tot}$ as low as possible (significantly less than 1) so that we could have a single photon detection with good signal-to-noise ratio.

We now look at how this parameter varies at various limits to analyse the behaviour at different operating regimes of the system. We do this by solving the master equation at these limits, from whose solutions we can calculate N_{prb}^{trans} and θ_p as explained in section 3.3.1. We substitute these values in the above equations

for calculating minimum time required to measure ($T_{Q/I}$) and the minimum number of signal photons required to measure ($N^{tot}_{sigQ/I}$).

3.5.2 Weak signal and weak probe limits

Similar to the calculations for the phase change in the probe, we start by getting analytical solutions for the weak signal and weak probe limit. As explained above, we first calculate the time taken to measure by taking signal-to-noise ratio SNR = 1. This gives,

$$T_Q = \frac{\left({\Gamma_s}^2 + 4\Delta \mathrm{s}^2\right)^2 \left({\Gamma_p}^2 + 4(\Delta \mathrm{p} + \Delta \mathrm{s})^2\right)^2}{64{\Gamma_p}^3{\Gamma_s}^4(\Delta \mathrm{p} + \Delta \mathrm{s})^2 N^{in}_{prb} {N^{in}_{sig}}^2},$$

and

$$T_I = \frac{\left({\Gamma_s}^2 + 4\Delta \mathrm{s}^2\right)^2 \left({\Gamma_p}^2 + 4(\Delta \mathrm{p} + \Delta \mathrm{s})^2\right)^2}{16{\Gamma_p}^5{\Gamma_s}^4 N^{in}_{prb} {N^{in}_{sig}}^2}.$$

To get a simplified solution, we substitute the values for detuning corresponding to the maximum phase shifts as given in eq.(3.3). We also consider the transmon limit with $\Gamma_p = 2\Gamma_s$ and check the behaviour at $N^{in}_{sig} = 0.005 \ll 1$.

With these values we have,

$$T_Q = \frac{10^4}{\Gamma_p N^{in}_{prb}},$$

and

$$T_I = \frac{9.9 \times 10^3}{\Gamma_p N^{in}_{prb}}.$$

The unit for the measurement times is set by Γ_p. With these measurement times we have the minimum number of signal photons required to make a detection as,

$$N^{tot}_{sigQ} = \frac{25}{N^{in}_{prb}},$$

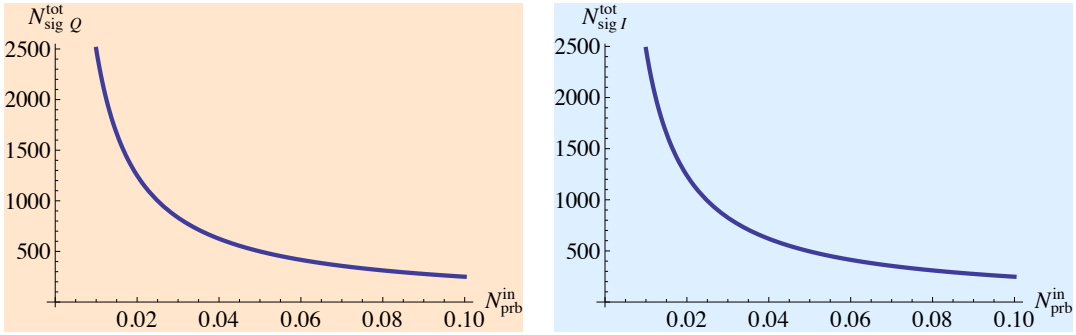

(a) (b)

Figure 3.7: Total number of signal photons to pass through the transmon before detection as a function of N^{in}_{prb} for a weak signal ($N^{in}_{sig} = 0.005$) and weak probe for (a) Quadrature measurement ($\theta_L = 0$) and (b) In-phase measurement ($\theta_L = \pi/2$).

and

$$N^{tot}_{sig\,I} = \frac{24.8}{N^{in}_{prb}}.$$

These values are plotted in Fig.3.7. From the figure, we see that the detection improves with higher probe strength, as higher probe strengths lead to shorter measurement time. But overall the value for N^{tot}_{sig} is very high in this regime, which is as expected. Since the signal strength is very weak, it takes significant number of signal photons to excite the transmon and have an impact on the probe photons. Apart from that, since the probe is also weak it takes significant time to make a measurement. Both of these factors result in larger values of N^{tot}_{sig} (much higher than 1).

3.5.3 Weak signal and strong probe limit

We next check the minimum time to measure for a weak signal but with a strong probe. We take the following limits to simplify the equation. We assume that we are in the transmon regime with $\Gamma_p = 2\Gamma_s$. We also take the signal to be on resonance with the 0-1 transition of the atom (i.e. Δs = 0) and the detuning of probe Δp = Γ_p. These values of the detunings correspond to maximum phase shift

as discussed in the section 3.4.2. This gives the minimum time to measure as,

$$T_Q = \frac{\left(25 + 12N_{prb}^{in}\right)^2 \left(5 + 8N_{prb}^{in}\left(1 + 2N_{prb}^{in}\right)\right)^2}{64\Gamma_p N_{prb}^{in}\left(25 + 28N_{prb}^{in}\right)^2 N_{sig}^{in\,2}},$$

and

$$T_I = \frac{\left(25 + 12N_{prb}^{in}\right)^2 \left(5 + 8N_{prb}^{in} + 16N_{prb}^{in\,2}\right)^2}{16\Gamma_p N_{prb}^{in}\left(25 + 36N_{prb}^{in}\right)^2 N_{sig}^{in\,2}}.$$

Taking the photon number range in this limit as $N_{sig}^{in} <= 0.005$ and $N_{prb}^{in} > 0.01$, we find that the minimum time required to make a measurement is at the maximum value of $N_{sig}^{in} = 0.005$. This is as expected because with stronger signal, we have larger phase change in the probe. With this limit of $N_{sig}^{in} = 0.005$, the minimum time to measure is given by,

$$T_Q = \frac{625\left(25 + 12N_{prb}^{in}\right)^2 \left(5 + 8N_{prb}^{in}\left(1 + 2N_{prb}^{in}\right)\right)^2}{\Gamma_p N_{prb}^{in}\left(25 + 28N_{prb}^{in}\right)^2},$$

and

$$T_I = \frac{2500\left(25 + 12N_{prb}^{in}\right)^2 \left(5 + 8N_{prb}^{in}\left(1 + 2N_{prb}^{in}\right)\right)^2}{\Gamma_p N_{prb}^{in}\left(25 + 36N_{prb}^{in}\right)^2}.$$

The number of signal photons to pass through the transmon in the above time is,

$$N_{sigQ}^{tot} = \frac{25\left(25 + 12N_{prb}^{in}\right)^2 \left(5 + 8N_{prb}^{in}\left(1 + 2N_{prb}^{in}\right)\right)^2}{16N_{prb}^{in}\left(25 + 28N_{prb}^{in}\right)^2},$$

and

$$N_{sigI}^{tot} = \frac{25\left(25 + 12N_{prb}^{in}\right)^2 \left(5 + 8N_{prb}^{in}\left(1 + 2N_{prb}^{in}\right)\right)^2}{4N_{prb}^{in}\left(25 + 36N_{prb}^{in}\right)^2}.$$

We plot the above equations in Fig.3.8 as a function of number of input probe photons.

From the graphs we see a minimum in N_{sig}^{tot} as given below with the corresponding value for N_{prb}^{in}

$$_{min}N_{sigQ}^{tot} = 297.946 \text{ at } N_{prb}^{in} \to 0.317582,$$

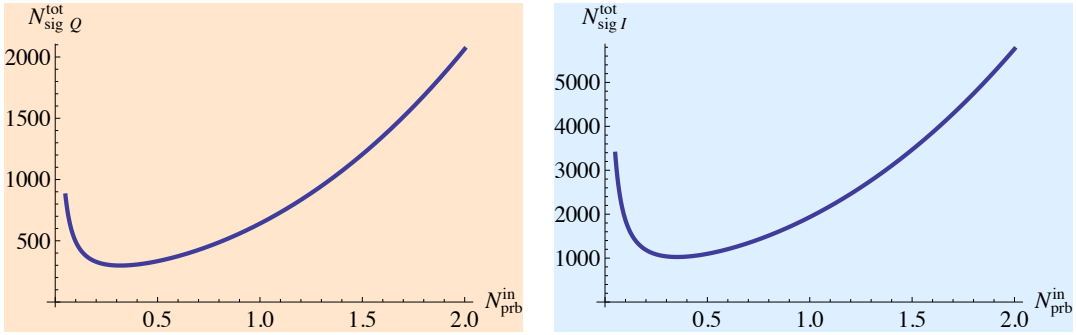

(a) (b)

Figure 3.8: Total number of signal photons to pass through the transmon before detection as a function of N^{in}_{prb} for a weak signal ($N^{in}_{sig} = 0.005$) and strong probe for (a) Quadrature measurement ($\theta_L = 0$) (b) In-phase measurement ($\theta_L = \pi/2$) .

and

$$_{min}N^{tot}_{sig\,I} = 1025.88 \text{ at } N^{in}_{prb} \to 0.351863.$$

Here again, we see that the values for $_{min}N^{tot}_{sig}$ are much higher than 1. In this case, the phase change in the probe will be less than in the previous regime, as a weak signal has significantly less impact on a stronger probe. Although initially, the measurement time reduces with the increase of probe strength (N^{in}_{prb}), we reach a minimum point after which the probe is so strong that it hardly feels the impact due to the presence of signal. This then results in the increase of N^{tot}_{sig} as shown in the figures.

3.5.4 Full Range Analysis

The aim of our calculations here is to find the minimum value for N^{tot}_{sig} by optimizing the parameters. If we have $N^{tot}_{sig} < 1$, then we have a single photon detector. As we can see from the above derivations in the weak limits, the value for N^{tot}_{sig} in those ranges is much larger than 1. In this section, we check how the value of N^{tot}_{sig} changes over the wide range of values for the parameters. Similar to our analysis of phase change, we first plot the variation of N^{tot}_{sig} as a function of different parameters.

The results are shown in Figs.3.9 - 3.11.

Next, we try to find the minimum of N_{sig}^{tot} with regards to Γ_s, Γ_p, Δs, Δp, N_{sig}^{in} and N_{prb}^{in} numerically. As the problem is unbounded, we set the range of value for N_{sig}^{in} and N_{prb}^{in} to be between 0.0001 and 3. Also, we assume to be in the transmon limit with Γ_p=2Γ_s. With this limit, we find that the minimum value for N_{sig}^{tot} as

$$_{min}N_{sigQ}^{tot} = 9.35743 \text{ for } N_{\text{sig}}^{in} \to 0.3,\ N_{\text{prb}}^{in} \to 3,\ \Delta\text{s} \to 0.49,\ \Delta\text{p} \to 1.36,\ \Gamma_s \to 0.4,$$

and

$$_{min}N_{sigI}^{tot} = 8.66717 \text{ for } N_{\text{sig}}^{in} \to 0.35,\ N_{\text{prb}}^{in} \to 0.23,\ \Gamma_s \to 2.59,\ \Delta\text{s} \to 0,\ \Delta\text{p} \to 0.$$

Although the above values are significant improvements from those we found in the weak limits, they are still greater than 1. From this, we come to the conclusion that single photon detection does not seem to be possible with this system. If we are to use this set-up as a detection mechanism, we would need to encode information in signal wave-packets of at least 9 photons. This motivates us to expand/modify our system as we are looking for a single photon detector. We do this in the next chapter, by adding more transmons in the transmission line to see if that would bring about any improvements to the problem.

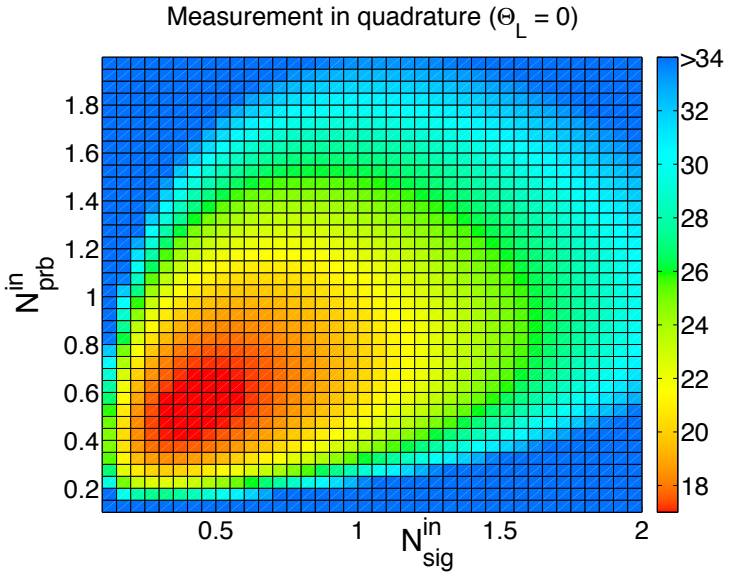

(a)

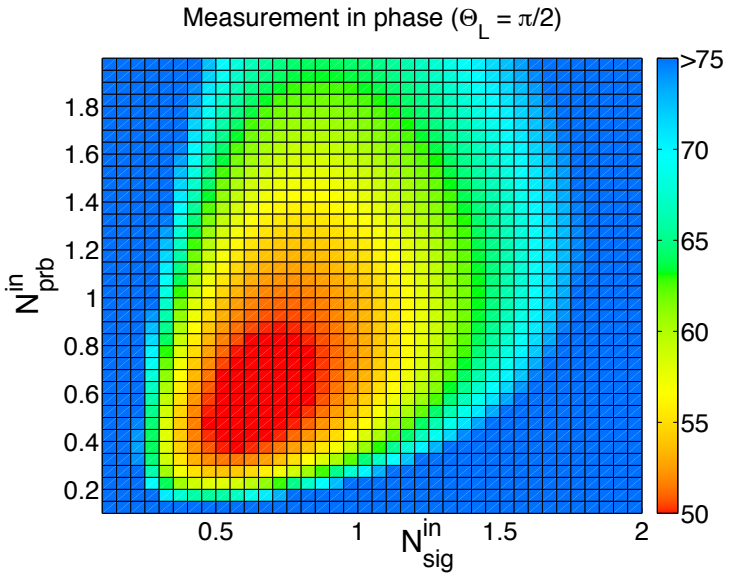

(b)

Figure 3.9: Total number of signal photons to pass through the transmon before detection as a function of N_{sig}^{in} and N_{prb}^{in} for (a)Quadrature measurement ($\theta_L = 0$) (b) In-phase measurement ($\theta_L = \pi/2$). The following values were assumed: $\Gamma_p = 2\Gamma_s$, $\Delta s = 0$ and $\Delta p = 2\Gamma_s$. From the graphs, we see that the optimum value for N_{sig}^{in} and N_{prb}^{in} is between 0.4 and 0.7 in both the cases.

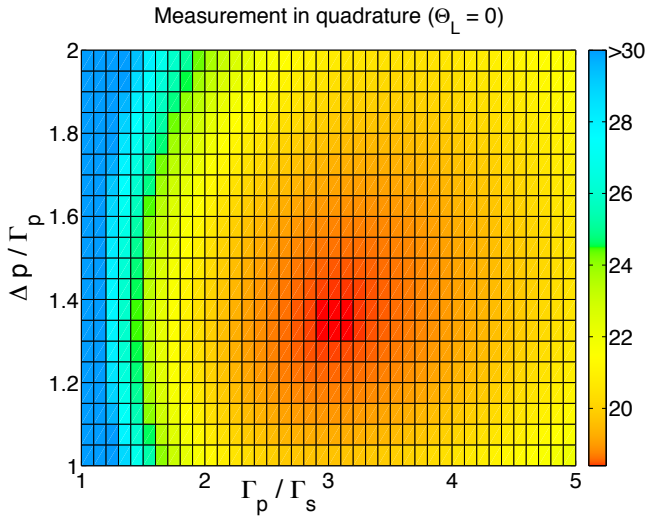

(a)

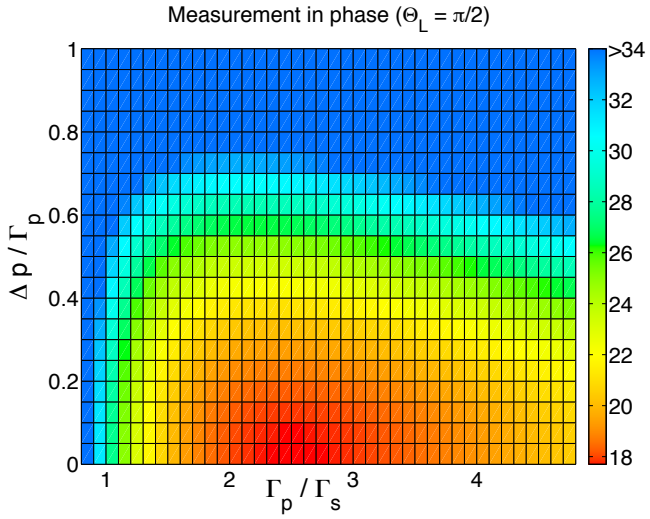

(b)

Figure 3.10: Total number of signal photons to pass through the transmon before detection as a function of Γ_p/Γ_s and $\Delta p/\Gamma_s$ with (a) Quadrature measurement (θ_L = 0) (b)In-phase measurement ($\theta_L = \pi/2$). The following values were assumed N_{sig}^{in}=1, N_{prb}^{in}=1, $\Delta s = 0$. For quadrature measurement we see that the optimum value for Δp is around Γ_p. This is consistent with our previous result that the maximum phase change in the probe occurs around this value. However, for in-phase measurement, we find the optimum value for Δp to be zero. As explained in Fig.3.4, at this value of Δp there is no phase change in the probe but here we see that there is a maximum reduction in amplitude at this value (In-phase measurement is dependent on the change of amplitude). This is possible if we have maximum loss at the value of Δp=0 (Refer Fig.3.15).

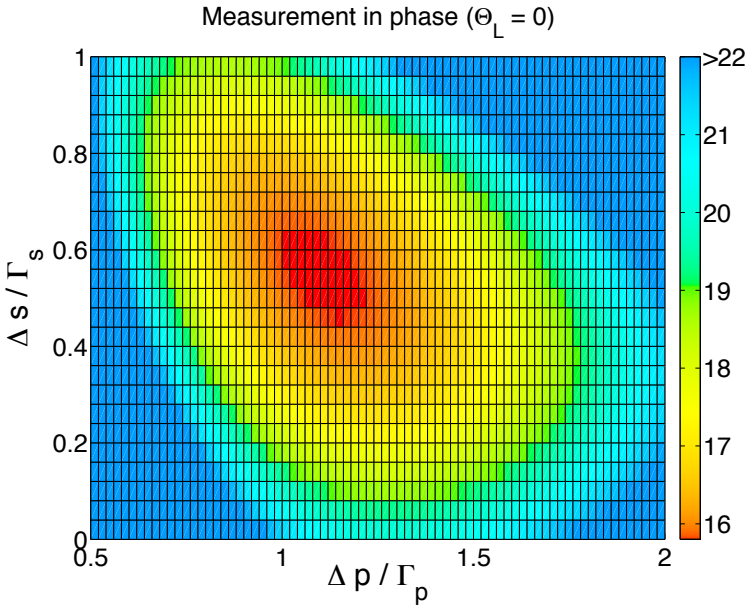

(a)

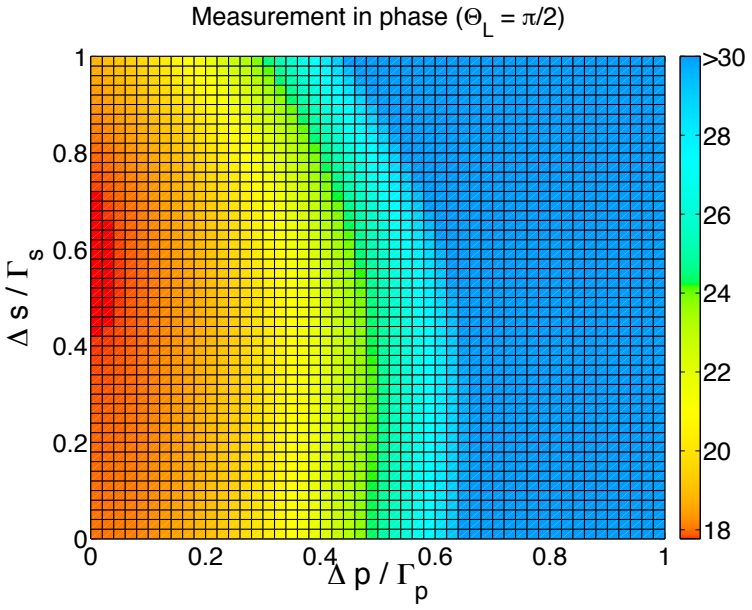

(b)

Figure 3.11: Total number of signal photons to pass through the transmon before detection as a function of $\Delta p/\Gamma_p$ and $\Delta s/\Gamma_s$ with (a) Quadrature measurement ($\theta_L = 0$) (b) In-phase measurement ($\theta_L = \pi/2$). The following values were assumed N^{in}_{sig}=1, N^{in}_{prb}=1 and Γ_p=2Γ_s. Here again we see that, for quadrature measurement the optimum value for $\Delta p \approx \Gamma_p$ while for in-phase measurement it is 0. For detuning in signal Δs, in both the cases the optimum value is around $0.5\Gamma_s$.

3.6 Losses

Comparing the graphs for the phase change in the probe (Fig 3.3 - 3.6) with graphs for minimum number of signal photons required to detect (Fig 3.9 - 3.11), we see that the optimum parameters for photon detection is not the same as the parameters for maximum phase change in the probe. This difference can be attributed to losses in the system which seem to play a significant role. There are two sources of losses in the system - reflection and incoherent scattering. As we are measuring only the transmitted probe field, the reflected probe photons are also taken as losses. The inchorent scattering occurs due to spontaneous emission of photons when the transmon is in the excited state. These photons do not have a definite frequency or phase.

Phase change in the probe and Losses

In this section, we see how the phase change in the probe and losses are related.

Fig 3.12 (a) shows the phase change in the probe as a function of the number of signal and probe photons per interaction time. Fig 3.12 (b) shows the loss % in the probe field given as

$$Loss_{prb}\% = \frac{N^{in}_{\mathrm{prb}} - N^{trans}_{\mathrm{prb}}}{N^{in}_{\mathrm{prb}}} \times 100,$$

where N^{in}_{prb} is the number of input probe photons per interaction time and N^{trans}_{prb} is the number of transmitted probe photons per interaction time. The calculations are done in the transmon limit i.e. with $\Gamma_p = 2\Gamma_s$. The values for the detunings are taken as $\Delta\mathrm{s} = 0$, $\Delta\mathrm{p} = \Gamma_p$. As shown in previous sections, these values correspond to the maximum phase shift.

From the comparison of the two figures, we see that at, the regions where we have large phase shifts we also have high losses. And low losses occur at regions with low phase shift. So, maximising the phase change may not be the way for

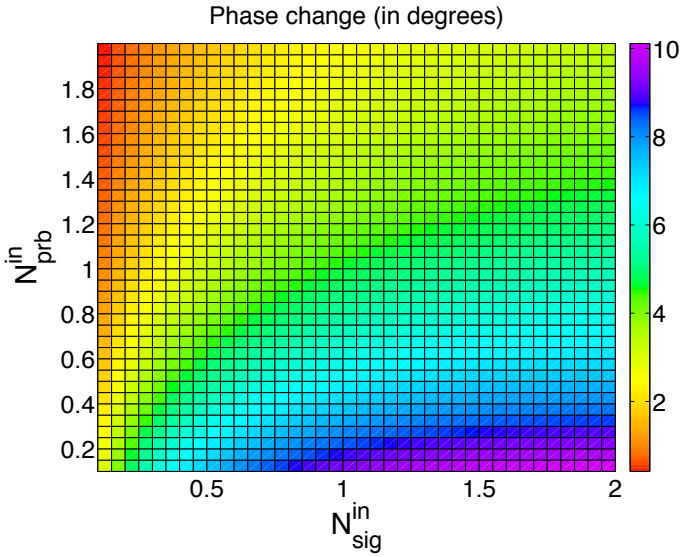

(a)

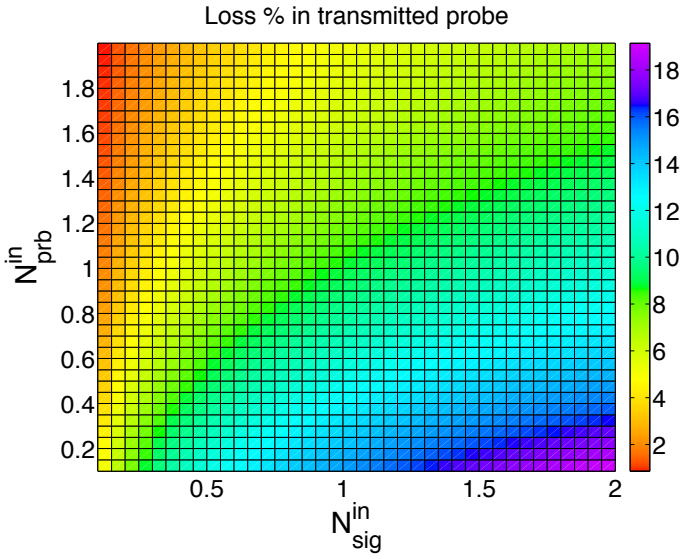

(b)

Figure 3.12: (a)Phase change in the probe (θ_p) in degrees and (b) Loss % of probe photons. The values of the other parameters are Δs = 0, Δp = Γ_p and $\Gamma_p = 2\Gamma_s$.

better photon detection.

Photon detection and Losses

The effect of losses on photon detection depends on the axis of measurement. The quadrature measurement as described in section 3.1, depends entirely on the phase change of the transmitted probe. If lesser probe photons get transmitted due to losses, it takes longer time to make a detection and hence would require higher N_{sig}^{tot}. However, this is not the case with in-phase detection. In this scenario, we are more interested in the change in the amplitude of the transmitted probe along this measurement axis. This change can come about by 2 ways - either through phase change or through losses. So loss actually helps the photon detection in the in-phase direction.

The above points are illustrated more in Fig.3.13. From the figure, we see the projection on Q axis with losses $A'_p sin(\theta_p)$ is less than the projection without losses $A_p sin(\theta_p)$, thus confirming that losses are bad for quadrature measurements. However, for in-phase measurements, it is the difference of transmitted probe field's strength with and without the signal that matters. From the figure we see that the difference in the projections in the I axis, with losses $Ap - A'_p cos(\theta_p)$ is larger than the one without losses $Ap - A_p cos(\theta_p)$. Thus, losses help in-phase photon detection and we conclude that there is an interplay between phase change and losses that needs to be taken into account with regards to photon detection.

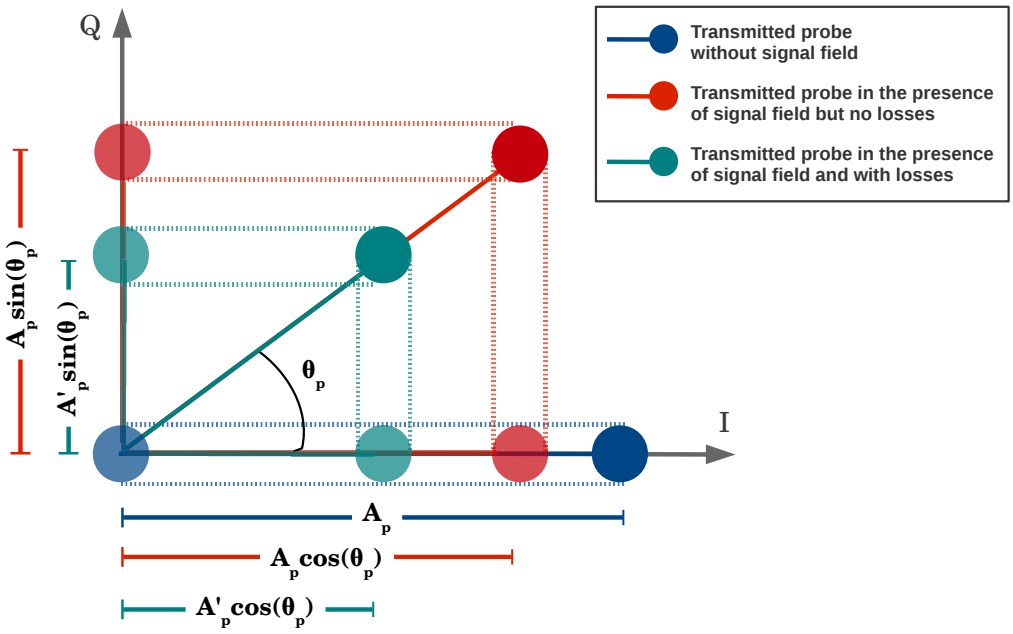

Figure 3.13: Effect of loss in the Homodyne detection.

Fig.3.14 shows the loss in probe field for the scenario when Δp=0. In this case, there is no phase change in the probe as explained in previous sections. But we also see that the loss in probe is significantly higher compared to the values in Fig.3.12(b). The effect of this loss seems to be much larger than the effect of maximum phase change(with losses) that can be achieved. This would explain why we see that the minimum number of signal photons to detect in-phase ${}_{min}N^{tot}_{sigI}$ to be slightly lower than for the measurement in quadrature ${}_{min}N^{tot}_{sigQ}$ in section 3.5.4.

In Fig.3.15, we further analyse the loss in transmitted probe as a function of probe detuning Δp and probe relaxation rate Γ_p. We find that, the maximum losses occur at Δp=0 as expected. This would substantiate our claim made in Fig.3.10(b), where we found that the minimum value for N^{tot}_{sigI} was with Δp=0. Since at this detuning, we have no phase change in the probe we attributed this to having maximum losses at this value. Indeed from the figure, we find that it is true.

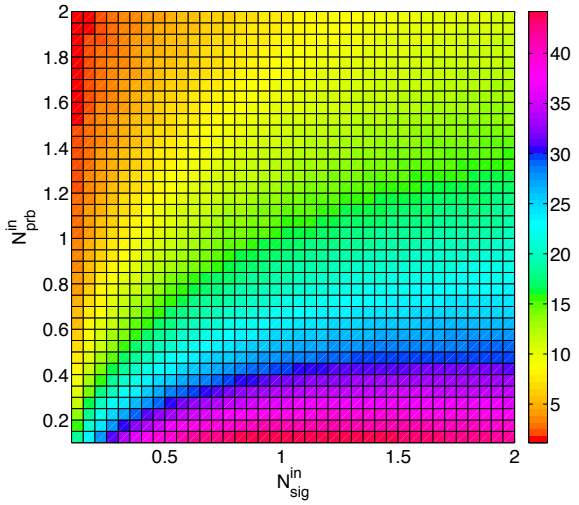

Figure 3.14: Loss % of transmitted probe photons with Δp=0. The values of the other parameters are Δs = 0 and $\Gamma_p = 2\Gamma_s$.

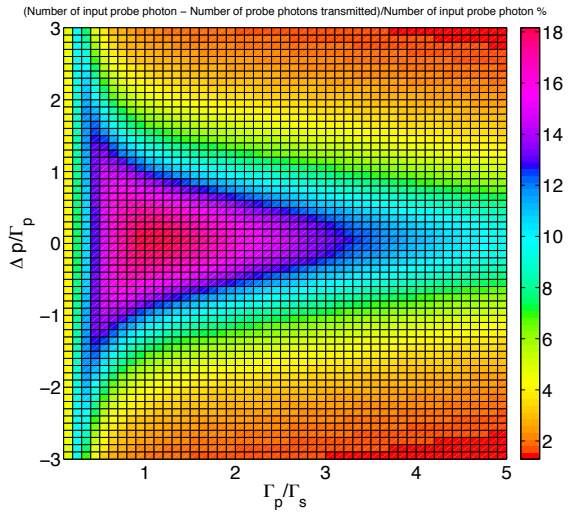

Figure 3.15: Loss % of transmitted probe photons as a function of Δp and Γ_p. The values of the other parameters are N^{in}_{sig}=1, N^{in}_{prb}=1 and Δs = 0.

3.6.1 Loss in the Signal field

In the above section, we discussed the losses in the probe field and how it affects photon detection. Since, the main concern of this thesis was to detect the signal photons by measuring probe photons, the losses in the signal field have not been analysed fully. Here, we want to mention that there are losses due to reflection and incoherent scattering in the signal field as well. This would mean that, the type of detection we are doing is not QND in the strict sense. However, we don't destroy the signal photons completely and there is a transmitted signal field that survives after detection which could be used for other quantum information processing tasks. Thus we have a non-destructive detection mechanism, where there is some loss in the signal field due to its interaction with the transmon. Further analysis is required to quantify these losses and to find operating regimes where the losses are minimum.

4

Multiple Transmons

In the previous chapter, we analysed the interaction of two coherent fields with a single transmon in a transmission line. From the analysis, we concluded that it does not seem possible to detect a single photon using the set-up presented. In this chapter, we extend the system further and analyse the interaction of two coherent fields with many transmons placed one after the other in the transmission line.

4.1 Cascaded quantum systems - No backscattering from the transmons

In this section, we consider the system shown in Fig.4.1 where we have many transmons one after another in the transmission line, but we don't have the reflections from a transmon getting back into the previous transmon. Practically, this can be achieved by inserting circulators between the transmons that would discard the reflected part. Such systems, where the output of one transmon is fed as the input to the next with no back scattering, are known as Cascaded Quantum Systems[34].

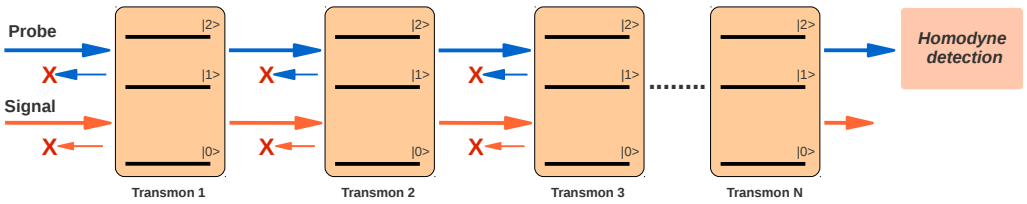

Figure 4.1: Set-up for multiple transmons on transmission line with no backscattering

4.1.1 Master equation

As with the case of a single transmon, we start with the master equation for the cascaded quantum system. To do this, we first derive the master equation for 2 transmons and then extend it to include N transmons.

Master equation for 2 transmons

Following [34], we derive the master equation for 2 transmons in the transmission line as follows

$$\begin{aligned}\dot{\rho} &= i\left[\rho, H_{\text{sys}}^{(1)} + H_{\text{sys}}^{(2)}\right] \\ &\quad + \frac{\gamma_s^{(1)}}{2}\mathcal{D}\left[\sigma_{01}^{(1)}\right]\rho + \frac{\gamma_p^{(1)}}{2}\mathcal{D}\left[\sigma_{12}^{(1)}\right]\rho + \frac{\gamma_s^{(2)}}{2}\mathcal{D}\left[\sigma_{01}^{(2)}\right]\rho + \frac{\gamma_p^{(2)}}{2}\mathcal{D}\left[\sigma_{12}^{(2)}\right]\rho \\ &\quad - \sqrt{\frac{\gamma_s^{(1)}}{2}\frac{\gamma_s^{(2)}}{2}}\mathcal{C}\left[\sigma_{01}^{(1)}, \sigma_{01}^{(2)}\right]\rho - \sqrt{\frac{\gamma_p^{(1)}}{2}\frac{\gamma_p^{(2)}}{2}}\mathcal{C}\left[\sigma_{12}^{(1)}, \sigma_{12}^{(2)}\right]\rho, \end{aligned} \tag{4.1}$$

where the superscripts represent the number of the transmon and the corresponding Hilbert space of the operators. Thus, we have

$$H_{\text{sys}}^{(1)} = H_{\text{sys}} \otimes 1_3 \ , \ H_{\text{sys}}^{(2)} = 1_3 \otimes H_{\text{sys}},$$

and

$$\sigma_{ij}^{(1)} = \sigma_{ij} \otimes 1_3 \ , \ \sigma_{ij}^{(2)} = 1_3 \otimes \sigma_{ij}.$$

The Hamiltonians $H_{\rm sys}^{(i)}$ contains the evolution of the transmons and their interaction with the two fields as given in eq.(2.3).

The dissipation and coupling super-operators are given by

$$\mathcal{D}\left[\hat{c}\right]\rho = \left(2\hat{c}\rho\hat{c}^\dagger - \hat{c}\rho\hat{c}^\dagger - \hat{c}\rho\hat{c}^\dagger\right),$$

and

$$\mathcal{C}\left[\hat{c_1},\hat{c_2}\right]\rho = \left\{\left[\hat{c_2}^\dagger,\hat{c_1}\rho\right] + \left[\rho\hat{c_1}^\dagger,\hat{c_2}\right]\right\}.$$

To make the equations simpler and to make the analysis easier, we will assume that all of the transmons that we consider are similar i.e both the transmons have same energy levels ($\omega_0^{(1)} = \omega_0^{(2)} = \omega_0$, $\omega_1^{(1)} = \omega_1^{(2)} = \omega_1$, $\omega_2^{(1)} = \omega_2^{(2)} = \omega_2$) and same coupling strengths ($\gamma_s^{(1)} = \gamma_s^{(2)} = \gamma_s$, $\gamma_p^{(1)} = \gamma_p^{(2)} = \gamma_p$).

The master equation then reduces to

$$\begin{aligned}\dot{\rho} &= \frac{i}{\hbar}\left[\rho, H_{\rm eff}\right] + \frac{\gamma_s}{2}\left(\mathcal{D}\left[\sigma_{01}^{(1)}\right]\rho + \mathcal{D}\left[\sigma_{01}^{(2)}\right]\rho - \mathcal{C}\left[\sigma_{01}^{(1)},\sigma_{01}^{(2)}\right]\rho\right) \\ &\quad + \frac{\gamma_p}{2}\left(\mathcal{D}\left[\sigma_{12}^{(1)}\right]\rho + \mathcal{D}\left[\sigma_{12}^{(2)}\right]\rho - \mathcal{C}\left[\sigma_{12}^{(1)},\sigma_{12}^{(2)}\right]\rho\right), \end{aligned} \tag{4.2}$$

where $H_{\rm eff} = H_{\rm sys}^{(1)} + H_{\rm sys}^{(2)} = H_{\rm sys} \otimes 1_3 + 1_3 \otimes H_{\rm sys}$. As with the single transmon case, to simplify the problem we go the rotating frame and apply the rotating wave approximation (RWA). Then we have,

$$\begin{aligned}\dot{\rho}^{rf} &= \frac{i}{\hbar}\left[\rho^{rf}, H_{\rm eff}^{rf}\right] + \frac{\gamma_s}{2}\left(\mathcal{D}\left[\sigma_{01}^{-(1)}\right]\rho^{rf} + \mathcal{D}\left[\sigma_{01}^{-(2)}\right]\rho^{rf} - \mathcal{C}\left[\sigma_{01}^{-(1)},\sigma_{01}^{-(2)}\right]\rho^{rf}\right) \\ &\quad + \frac{\gamma_p}{2}\left(\mathcal{D}\left[\sigma_{12}^{-(1)}\right]\rho^{rf} + \mathcal{D}\left[\sigma_{12}^{-(2)}\right]\rho^{rf} - \mathcal{C}\left[\sigma_{12}^{-(1)},\sigma_{12}^{-(2)}\right]\rho^{rf}\right), \end{aligned} \tag{4.3}$$

where $H_{\rm eff}^{rf} = \sum_{j=1}^{2} H_{\rm sys}^{rf(j)} = H_{\rm sys}^{rf} \otimes 1_3 + 1_3 \otimes H_{\rm sys}^{rf}$ with $H_{\rm sys}^{rf}$ being the same as in eq.(2.12). Similarly, we have $\sigma_{ij}^{-(1)} = \sigma_{ij}^{(-)} \otimes 1_3$, $\sigma_{ij}^{-(2)} = 1_3 \otimes \sigma_{ij}^{(-)}$ with the values

of σ_{ij}^{-} given in eq.(3.1).

Master equation for N transmons

From the above equation, it is straight forward to generalize to N similar transmons set-up depicted in Fig.4.1. The master equation is then given by,

$$\begin{aligned}\dot{\rho}^{rf} &= i\left[\rho^{rf}, H_{\text{eff}}^{rf}\right] + \frac{\gamma_s}{2}\left(\sum_{j=1}^{N}\mathcal{D}\left[\sigma_{01}^{-(j)}\right]\rho - \sum_{j=1}^{N}\sum_{k=j+1}^{N}\mathcal{C}\left[\sigma_{01}^{-(j)}, \sigma_{01}^{-(k)}\right]\rho\right) \\ &\quad + \frac{\gamma_p}{2}\left(\sum_{j=1}^{N}\mathcal{D}\left[\sigma_{12}^{-(j)}\right]\rho - \sum_{j=1}^{N}\sum_{k=j+1}^{N}\mathcal{C}\left[\sigma_{12}^{-(j)}, \sigma_{12}^{-(k)}\right]\rho\right), \end{aligned} \tag{4.4}$$

where $H_{\text{eff}}^{rf} = \sum_{j=1}^{N} H_{\text{sys}}^{rf(j)}$ with H_{sys}^{rf} being the same as in eq.(2.12) and the σ^{-} operators are given in eq.(3.1).

Solutions of the master equation

Similar to the single transmon case, the master equation is solved to find the steady state density matrix ρ^{ss} of the system. Considering only coherent output fields, we average the fields radiated from the last transmon. In units of frequency, this is given as

$$\Omega_s^{rad} = i\Gamma_s < \sigma_{01}^{-(N)} >= i\Gamma_s\, tr(\rho^{ss}\sigma_{01}^{-(N)}), \tag{4.5}$$

and

$$\Omega_p^{rad} = i\Gamma_p < \sigma_{12}^{-(N)} >= i\Gamma_p\, tr(\rho^{ss}\sigma_{12}^{-(N)}). \tag{4.6}$$

The output fields after N transmons is similar to the one transmon case which is given by

$$\Omega_s^{trans} = \Omega_s + \Omega_s^{rad} = |\Omega_s^{trans}|e^{\mathrm{i}\theta_s},$$

and

$$\Omega_p^{trans} = \Omega_p + \Omega_p^{rad} = |\Omega_p^{trans}|e^{\mathrm{i}\theta_p},$$

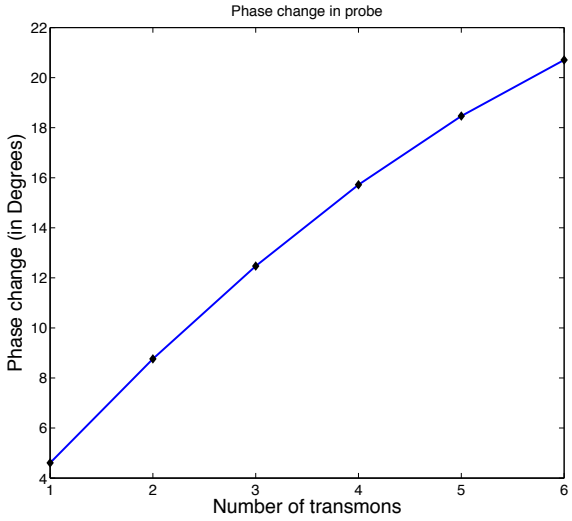

Figure 4.2: Phase change in the probe after each transmon. The value of the parameters were taken to be $N_{sig}^{in} = 1$, $N_{prb}^{in} = 1$, $\Delta s = 0$, $\Delta p = \Gamma_p = 2\Gamma_s$.

where $\Omega_{s/p}$ are the Rabi frequencies of the input drives as given in eq.(2.6).

4.1.2 Phase change in the probe

We first consider how the phase change in the probe θ_p varies with addition of each transmon by solving the master equation shown above. The result is shown in Fig.4.2. As we can see from the graph, the phase change in the probe increases with the addition of each transmon in the transmission line. However, the increase is not linear and we expect to reach a saturation after certain number of transmons. This would give a maximum phase change that could be achieved for a particular set of input parameters. The saturation limit is set by the losses in the system. As the signal and probe fields interact with each transmons, some parts of them are reflected and some are lost incoherently. Thus, with each addition of a transmon, the signal strength becomes weaker and the phase change it can impart on the probe becomes reduced.

4.1.3 Photon Detection

As we see from the previous section, addition of transmons improves the phase change in the probe. Here, we check to see if this set-up can improve photon detection as well. Fig.4.3 shows the variation of minimum number of signal photons required to make a detection (N_{sig}^{tot}) with addition of each transmon.

From the figures, we see that there is a clear improvement in photon detection with addition of transmons. Similar to the case of phase change, we expect to see a saturation in the improvements after certain number of transmons. This can be again attributed to losses. Since we have losses in both the signal and the probe fields, not only the phase change in the probe reduces but also the strength of the probe field transmitted at the end of the transmon chain also reduces. As discussed in the case of single transmons, the reduction of probe strength implies longer measurement times and hence more signal photons would have passed through the transmons during this period.

Most interestingly, we also see that with the in-phase measurement, we could achieve single photon detection after 6 transmons (See Fig.4.3(b)).The value of N_{sig}^{tot} at this point is 0.9559 which is indeed less than 1. The simulations were performed with a first set of values for the parameters. With further optimization, we should be able to go to lower values of N_{sig}^{tot}, which would imply that we can have single photon detection with good signal-to-noise ratio (SNR).

4.2 Other scenarios

Since we found that addition of more transmons can improve phase change in the probe and also photon detection, we consider other ways of connecting the multiple transmons and see if they give further improvements. These scenarios are described below along with the corresponding master equations where, to simplify the problem we have assumed that all the transmons to be similar. The master

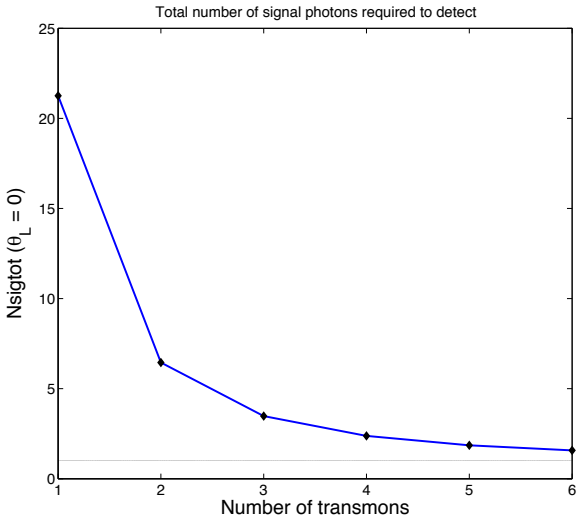

(a)

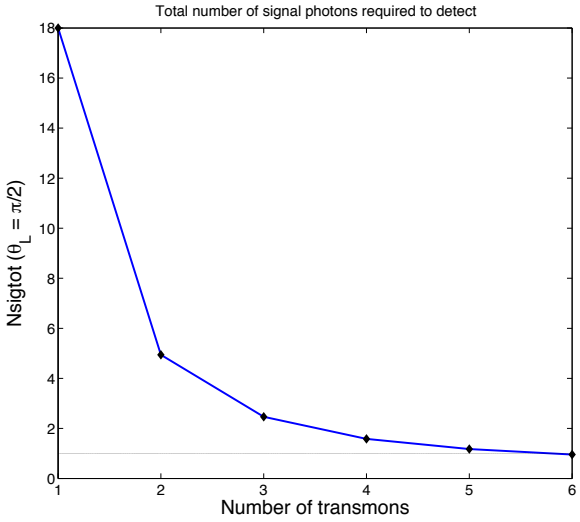

(b)

Figure 4.3: Total number of signal photons to pass through the transmons before detection as a function of number of transmons for (a)Quadrature measurement (θ_L = 0) with Δp = Γ_p (b) In-phase measurement ($\theta_L = \pi/2$) with Δp = 0. The value of the other parameters were taken to be $N^{in}_{sig} = 1$, $N^{in}_{prb} = 1$,Γ_p=2Γ_s and Δs = 0.

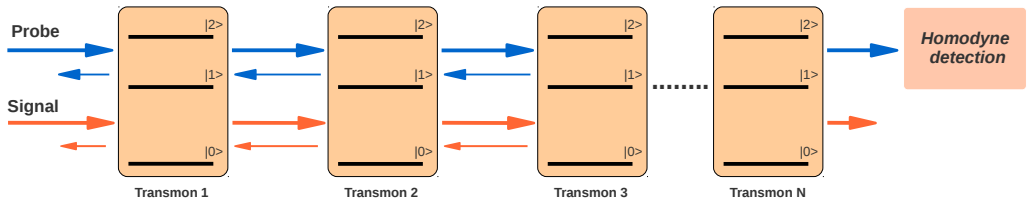

Figure 4.4: Set-up for multiple transmons on transmission line with backscattering

equations are derived in reference [36]. Here, we take these master equations as the starting point and solve them, to find the phase change in the probe (θ_p) and the minimum number of signal photons required to make detection (N_{sig}^{tot}) as in the previous case.

4.2.1 With backscattering in both signal and probe

In this case, we allow the reflections of the signal and probe field from the transmon to interact with the previous transmons. This situation is schematically shown in Fig.4.4. This is more straight-forward to implement experimentally as there is no need of other devices such as circulators in between the transmons. The master equation in this case is,

$$\dot{\rho}^{rf} = i\left[\rho^{rf}, H_{\text{eff}}^{rf}\right] + \frac{\gamma_s}{2}\mathcal{D}\left[\sum_{j=1}^{N}\sigma_{01}^{-(j)}\right]\rho^{rf} + \frac{\gamma_p}{2}\mathcal{D}\left[\sum_{j=1}^{N}\sigma_{12}^{-(j)}\right]\rho^{rf}, \quad (4.7)$$

where $H_{\text{eff}}^{rf} = \sum_{j=1}^{N} H_{\text{sys}}^{rf(j)}$ with H_{sys}^{rf} being the same as in eq.(2.12) and the σ^- operators are given in eq.(3.1). The equations for the fields radiated from the last transmon are the same as in eqs.(4.5) -(4.6).

4.2.2 With backscattering in only one field

This scenario is a combination of the previous two scenarios where we allow reflection from only one of the field (signal/probe) to go back to the previous transmon. We envision that this could be achieved with a circulator that would throw away one of the reflected fields based on the frequency. The master equations in these two cases are given below:

With backscattering only in signal

$$\begin{aligned}\dot{\rho}^{rf} &= i\left[\rho^{rf}, H_{\text{eff}}^{rf}\right] + \frac{\gamma_s}{2}\mathcal{D}\left[\sum_{j=1}^{N}\sigma_{01}^{-(j)}\right]\rho^{rf} \\ &\quad + \frac{\gamma_p}{2}\left(\sum_{j=1}^{N}\mathcal{D}\left[\sigma_{12}^{-(j)}\right]\rho^{rf} - \sum_{j=1}^{N}\sum_{k=j+1}^{N}\mathcal{C}\left[\sigma_{12}^{-(j)}, \sigma_{12}^{-(k)}\right]\rho^{rf}\right). \end{aligned} \tag{4.8}$$

With backscattering only in probe

$$\begin{aligned}\dot{\rho}^{rf} &= i\left[\rho^{rf}, H_{\text{eff}}^{rf}\right] + \frac{\gamma_s}{2}\left(\sum_{j=1}^{N}\mathcal{D}\left[\sigma_{01}^{-(j)}\right]\rho^{rf} - \sum_{j=1}^{N}\sum_{k=j+1}^{N}\mathcal{C}\left[\sigma_{01}^{-(j)}, \sigma_{01}^{-(k)}\right]\rho^{rf}\right) \\ &\quad + \frac{\gamma_p}{2}\mathcal{D}\left[\sum_{j=1}^{N}\sigma_{12}^{-(j)}\right]\rho^{rf}. \end{aligned} \tag{4.9}$$

Here again, we have $H_{\text{eff}}^{rf} = \sum_{j=1}^{N} H_{\text{sys}}^{rf(j)}$ with H_{sys}^{rf} being the same as in eq.(2.12) and the σ^- operators are given in eq.(3.1). The equations for the fields radiated from the last transmon are same as in eqs.(4.5) - (4.6).

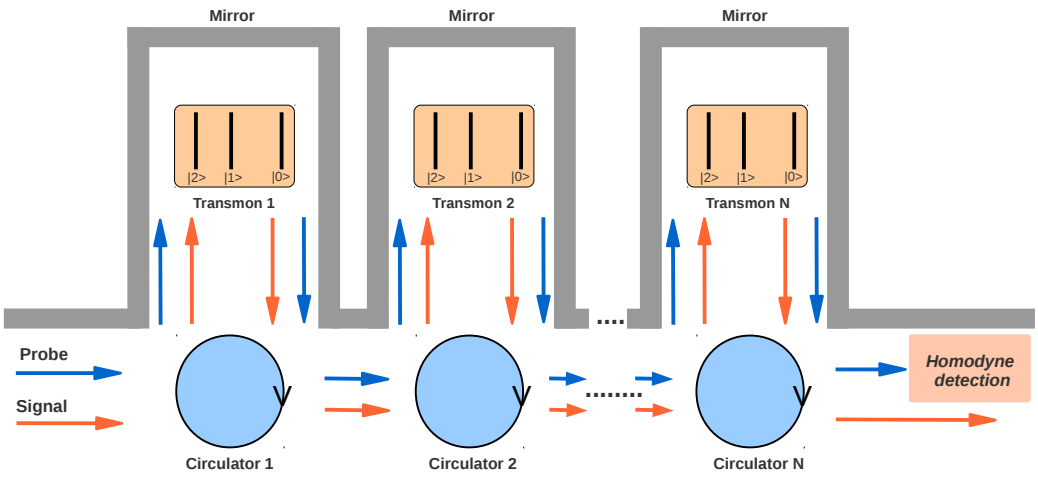

Figure 4.5: Set-up for multiple transmons on transmission line with mirrors

4.2.3 With a mirror at each transmon

The final scenario that we consider is that of having a superconducting mirror at each transmon. This is shown schematically in Fig.4.5. The circulators route the incoming fields to the transmons placed in front of a mirror. The transmitted and the reflected fields from the transmon get added and are routed to the next transmon by the circulators. Thus, the reflected fields are also collected and forwarded to the next transmon, reducing the losses.

The master equation in this case is,

$$\begin{aligned}\dot{\rho}^{rf} &= i\left[\rho^{rf}, H^{rf}_{\text{eff}}\right] + \frac{\gamma_s}{2}\left(\sum_{j=1}^{N}\mathcal{D}\left[\sigma_{01}^{-(j)}\right]\rho^{rf} - 2\sum_{j=1}^{N}\sum_{k=j+1}^{N}\mathcal{C}\left[\sigma_{01}^{-(j)}, \sigma_{01}^{-(k)}\right]\rho^{rf}\right) \\ &+ \frac{\gamma_p}{2}\left(\sum_{j=1}^{N}\mathcal{D}\left[\sigma_{12}^{-(j)}\right]\rho^{rf} - 2\sum_{j=1}^{N}\sum_{k=j+1}^{N}\mathcal{C}\left[\sigma_{12}^{-(j)}, \sigma_{12}^{-(k)}\right]\rho^{rf}\right), \end{aligned} \tag{4.10}$$

where we have $H^{rf}_{\text{eff}} = \sum_{j=1}^{N} H^{rf(j)}_{\text{mirror}}$. The equation for H^{rf}_{mirror} is different from the previous cases as the mirror introduces a renormalization in the coupling strengths.

The Hamiltonian in this case is given by,

$$H^{rf}_{mirror} = \begin{pmatrix} -\Delta\mathrm{s} & 0 & 0 \\ 0 & 0 & 0 \\ 0 & 0 & \Delta\mathrm{p} \end{pmatrix} + \Gamma_s\sqrt{N^{in}_{sig}} \begin{pmatrix} 0 & 1 & 0 \\ 1 & 0 & 0 \\ 0 & 0 & 0 \end{pmatrix} + \Gamma_p\sqrt{N^{in}_{prb}} \begin{pmatrix} 0 & 0 & 0 \\ 0 & 0 & 1 \\ 0 & 1 & 0 \end{pmatrix}. \tag{4.11}$$

Also the fields radiated by the last transmon in this case are modified as,

$$\Omega^{rad}_s = i\sqrt{2}\Gamma_s < \sigma^{-(N)}_{01} >= i\sqrt{2}\Gamma_s\, tr(\rho^{ss}\sigma^{-(N)}_{01}), \tag{4.12}$$

and

$$\Omega^{rad}_p = i\sqrt{2}\Gamma_p < \sigma^{-(N)}_{12} >= i\sqrt{2}\Gamma_p\, tr(\rho^{ss}\sigma^{-(N)}_{12}). \tag{4.13}$$

4.3 Simulation and comparison of the scenarios

We simulate the above master equations using Matlab. In these simulations, similar to the previous cases, we solve for the output probe field after N transmons for some given parameters. From this, we calculate the number of probe photons transmitted and the phase change in the probe after N transmons. We then plug-in these values in the formula for signal-to-noise ratio (SNR) as described in section 3.5.1 to calculate the measurement times ($T_{Q/I}$) and the minimum number of signal photons($N^{tot}_{sigQ/I}$) required to measure.

Figs. 4.6, 4.7 and 4.8 show the variation in the minimum number of signal photons required to detect in phase, in quadrature and the phase change in the probe for all of the above scenarios. From the graphs, we can see that having a mirror at each transmon is the most promising scenario for maximising phase change and hence for photon detection in quadrature. We can attribute this to the minimization of losses as the mirrors collect the fields reflected from the transmon and forward them to the next transmon.

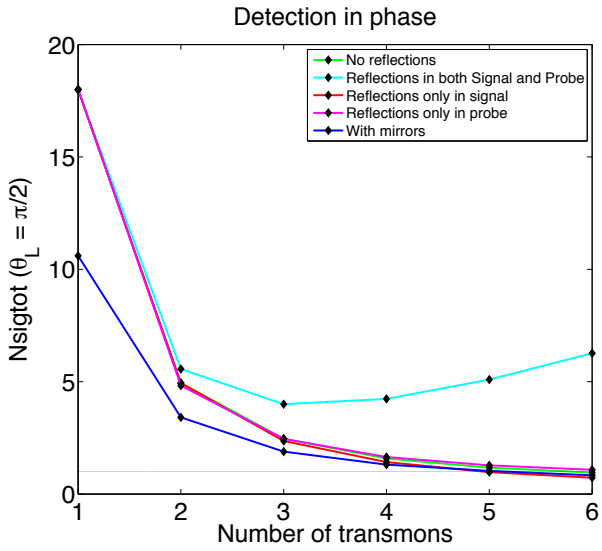

Figure 4.6: Number of signal photons required to make a detection in phase as a function of the number of transmons. The values of the parameters are $N_{\text{sig}}^{\text{in}} = 1, N_{\text{prb}}^{\text{in}} = 1, \Delta s = 0, \Delta p = 0, \Gamma_p = 2\Gamma_s$. Minimum value of 0.7284 is reached after 6 transmons for the scenario where reflections are allowed only in signal.

In the case of in-phase measurement, we see that the scenario of allowing reflections only in the signal is better than the other scenarios. Since we have simulated with the parameter Δp=0, phase change doesn't play a role in this case and only losses contribute to the reduction of amplitude of the transmitted probe. Thus we see that it is better to throw away the reflected probe fields. As the signal fields contain information that we are trying to detect, keeping the reflected part from the signal alone helps.

Strangely, when we allow for reflections in both the signal and probe fields, we see a degradation in performance with addition of more transmons. Further investigation is required to understand the causes for this behaviour.

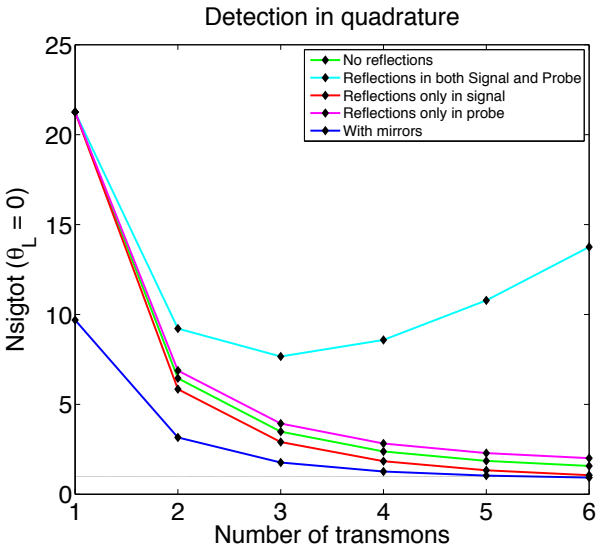

Figure 4.7: Number of signal photons required to make a detection in the quadrature as a function of the number of transmons. The values of the parameters are $N_{\text{sig}}^{\text{in}} = 1$, $N_{\text{prb}}^{\text{in}} = 1$, $\Delta s = 0$, $\Delta p = \Gamma_p = 2\Gamma_s$. The minimum value of 0.9245 is reached after 6 transmons when we have a mirror at each transmon.

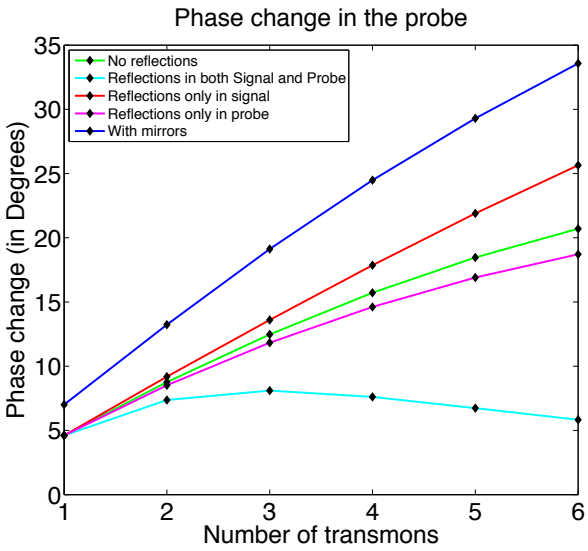

Figure 4.8: Phase change in the probe as a function of the number of transmons. The values of the parameters are $N_{\text{sig}}^{\text{in}} = 1$, $N_{\text{prb}}^{\text{in}} = 1$, $\Delta s = 0$, $\Delta p = \Gamma_p = 2\Gamma_s$. Maximum value of 33.5722 ° is reached after 6 transmons for the scenario where we have a mirror at each transmon.

4.4 Optimization of the parameters

As explained before, the results in the previous section are with the initial set of parameters and are not the optimum values. To find the optimum values for the parameters, we consider the two most promising scenarios; i.e. that of having multiple transmons with reflections allowed only for the signal and the one with mirror at each transmon.

4.4.1 With reflections only in signal

First we consider the scenario where we allow reflections only in the signal field to interact with the previous transmons and block the reflected probe field. As seen in the previous section, this seemed to be the most promising when measuring in phase. Hence, in this section we verify how the value of N_{sigI}^{tot}, the minimum number of signal photons required to make a detection in phase, varies with the change of parameters.

Fig.4.9 shows the variation of N_{sigI}^{tot} after 6 transmons as a function of the input signal and probe field strengths. The minimum value achieved was N_{sigI}^{tot}=0.6816, which corresponds to a signal-to-noise ratio(SNR) of 1.46 for single photon detection.

Fig.4.10 shows the variation of N_{sigI}^{tot} after 6 transmons as the function of probe detuning Δp and probe relaxation rate Γ_p. From the figure we see that the optimum values are obtained when Δp=0 as expected. We also see that it is better to be in the regime with higher value of the ratio Γ_p/Γ_s with the optimum value of this ratio being 4. The minimum value in this case was found to be N_{sigI}^{tot}=0.6111, which corresponds to SNR=1.64 for single photon detection.

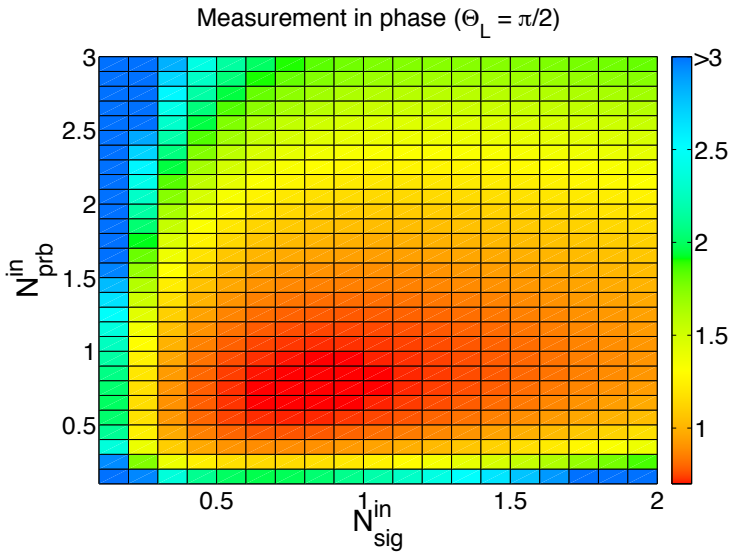

Figure 4.9: Number of signal photons required to make a detection in phase after 6 transmons for the scenario with reflections only in signal with $\Delta s = 0$, $\Delta p = 0$, $\Gamma_p = 2\Gamma_s$. Minimum value = 0.6816 at $N^{in}_{sig} = 0.8$, $N^{in}_{prb} = 0.7$.

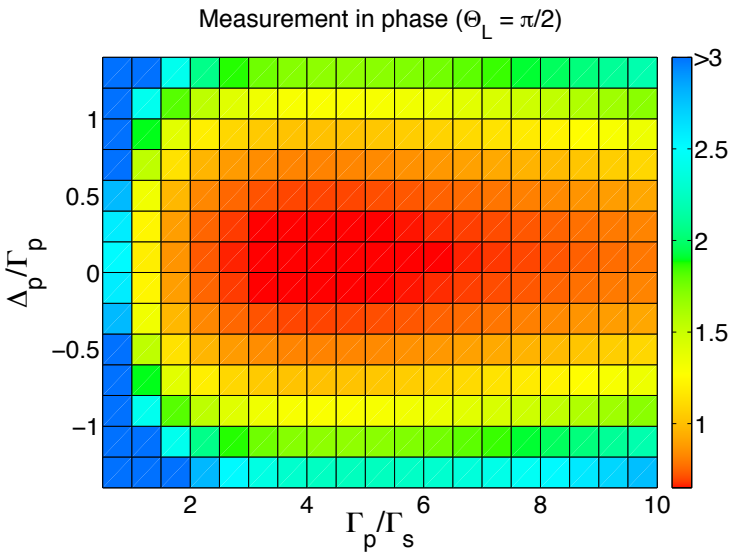

Figure 4.10: Number of signal photons required to make a detection in phase after 6 transmons for the scenario with reflections only in signal with $N^{in}_{sig} = 1$, $N^{in}_{prb} = 1$, $\Delta s = 0$. Minimum value = 0.6111 at $\Delta p = 0$, $\Gamma_p/\Gamma_s = 4$.

4.4.2 With a mirror at each transmon

Next we consider the case of having a mirror at each transmon. From the previous section, we see that this scenario is most promising in order to maximise the phase change in the probe and to measure in quadrature. Thus, in this section we see how the phase change in the probe θ_p and the minimum number of signal photons required to measure in quadrature (N^{tot}_{sigQ}) vary with the parameters for this scenario.

In Fig.4.11, we plot the change of N^{tot}_{sigQ} after 6 transmons as a function of input signal and probe powers. From the figure, we see that in this situation it is better to be in the lower powers of the input fields. A minimum value of N^{tot}_{sigQ}=0.2555 is achieved when $N^{\text{in}}_{\text{sig}} = 0.1$, $N^{\text{in}}_{\text{prb}} = 0.3$. This would correspond to a signal-to-noise ratio (SNR) of 3.9 for a single photon detection.

We plot the variation of phase change in the probe (θ_p) after 6 transmons as a function of the input field powers in Fig.4.12. As expected, we see that the maximum phase change occurs when the probe power is the lowest. But we also see that the maximum phase shift occurs when $N^{\text{in}}_{\text{sig}} = 1$ and then goes down. This has to be further investigated to find the cause for this reduction of phase change with increasing signal strength. The maximum phase change that is obtained is around 108 degrees. This is much higher compared to the typical values of 10^{-6} degrees achieved in nonlinear photonic crystal fibres [37, 38].

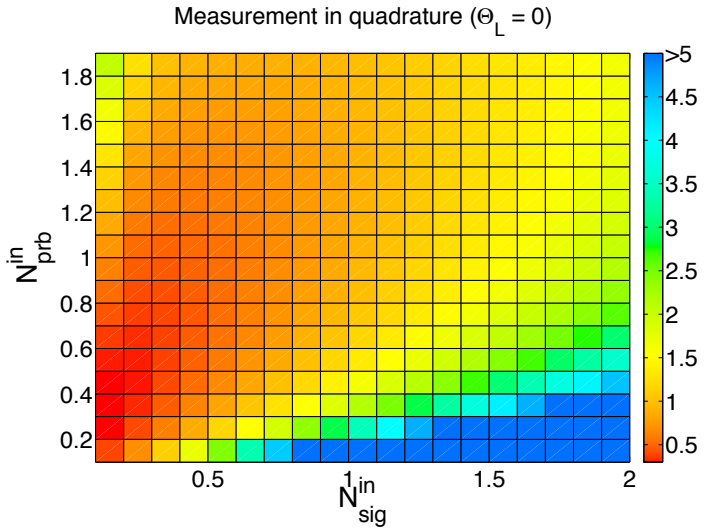

Figure 4.11: Number of signal photons required to make a detection in quadrature after 6 transmons for the scenario with mirrors with $\Delta s = 0$, $\Delta p = \Gamma_p = 2\Gamma_s$. Minimum value=0.2555 at $N^{in}_{sig} = 0.1$, $N^{in}_{prb} = 0.3$.

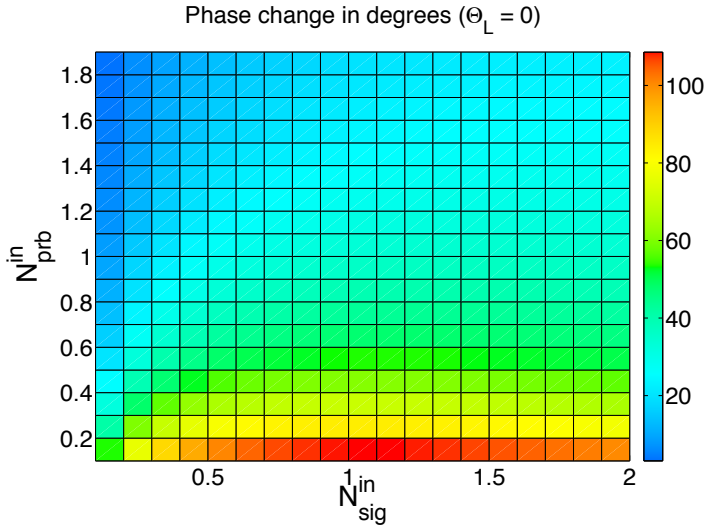

Figure 4.12: Phase change (in degrees) in the probe after 6 transmons for the scenario with mirrors with $\Delta s = 0$, $\Delta p = \Gamma_p = 2\Gamma_s$. Maximum value of the phase change in the probe θ_p=108.6012° at $N^{in}_{sig} = 1$, $N^{in}_{prb} = 0.1$.

5

Conclusions and Outlook

In this thesis, we looked at the possibilities of doing a non-destructive detection of a propagating microwave photon using the cross-Kerr effect by having an artificial atom (transmon) in a transmission line. To this extent, we introduced the Hamiltonian of the system and the master equation formalism. We also introduced the relevant parameters to analyse such as the phase change in the probe θ_p and the minimum number of signal photons required to make a detection N_{sig}^{tot}.

With a single transmon, we first looked at the phase change in probe and how it behaved under various regimes. We also explored the parameter space to find the optimum values for the minimum number of signal photons required to make a detection (N_{sig}^{tot}) and found it be around 9 in the transmon regime. We also looked at the significant role that losses seem to play in this regards.

We expanded the physical set-up to include many transmons in the transmission line. We looked at different scenarios, to analyse if any of those configurations would help our case of photon detection and the case of maximising the phase change in probe. Indeed, we found few operating regimes where we could get down to single photon detection with good signal to noise ratio (Best value as of

date: $N_{sig}^{tot} = 0.2555$ corresponding to SNR of 3.9 for single photon detection for the scenario of having a mirror at each transmon). We also found parameters for getting quite high phase change in the probe by having a mirror at each transmon (Best value as of date: $\theta_p = 108\,^\circ$).

Although we have interesting results that would solve the problem of photon detection, there is scope for lot of work in the future. With regards to the single transmon case, we would like to find out the physics at the fundamental level that sets the limits for photon detection at around 9 photons. This would help us to gain insight not only on this problem but also to understand the multiple transmon cases.

In the multiple transmon scenario, as can be seen from the figures, we have simulated only till the case of having 6 transmons in the transmission line. This constraint was set by the computational resources. We would like to extend the simulations to include more transmons. This would help us to find the global maximum phase change that could be achieved and the global minimum of the number of signal photons required to make a detection.

This thesis work was done with the assumption of being at the temperature of 0 K. To get experimentally relevant values, we also need to include the effect of temperature and add pure dephasing to the system.

Finally, it has to be noted that the kind of detection we have verified is not QND in the strict sense. Although we haven't destroyed the signal photons by directly detecting it, there are still losses due to reflection and incoherent scattering. So the transmitted signal is not the same as the input signal and would have been reduced in amplitude. Further analysis is required to see how much of the signal is lost and how it can be reduced by tuning the parameters.

Bibliography

[1] C. Monroe, Quantum information processing with atoms and photons, Nature 416 (6877) (2002) 238–246.
URL http://dx.doi.org/10.1038/416238a

[2] J. Clarke, F. K. Wilhelm, Superconducting quantum bits, Nature 453 (7198) (2008) 1031–1042.
URL http://dx.doi.org/10.1038/nature07128

[3] R. J. Schoelkopf, S. M. Girvin, Wiring up quantum systems, Nature 451 (7179) (2008) 664–669.
URL http://dx.doi.org/10.1038/451664a

[4] A. Wallraff, D. I. Schuster, A. Blais, L. Frunzio, R.-S. Huang, J. Majer, S. Kumar, S. M. Girvin, R. J. Schoelkopf, Strong coupling of a single photon to a superconducting qubit using circuit quantum electrodynamics, Nature 431 (7005) (2004) 162–167.
URL http://dx.doi.org/10.1038/nature02851

[5] A. A. Houck, D. I. Schuster, J. M. Gambetta, J. A. Schreier, B. R. Johnson, J. M. Chow, L. Frunzio, J. Majer, M. H. Devoret, S. M. Girvin, R. J. Schoelkopf, Generating single microwave photons in a circuit, Nature 449 (7160) (2007) 328–331.
URL http://dx.doi.org/10.1038/nature06126

[6] D. I. Schuster, A. A. Houck, J. A. Schreier, A. Wallraff, J. M. Gambetta, A. Blais, L. Frunzio, J. Majer, B. Johnson, M. H. Devoret, S. M. Girvin, R. J. Schoelkopf, Resolving photon number states in a superconducting circuit, Nature 445 (7127) (2007) 515–518.
URL http://dx.doi.org/10.1038/nature05461

[7] L. DiCarlo, J. M. Chow, J. M. Gambetta, L. S. Bishop, B. R. Johnson, D. I. Schuster, J. Majer, A. Blais, L. Frunzio, S. M. Girvin, R. J. Schoelkopf, Demonstration of two-qubit algorithms with a superconducting quantum processor, Nature 460 (7252) (2009) 240–244.
URL http://dx.doi.org/10.1038/nature08121http://www.nature.com/nature/journal/v460/n7252/suppinfo/nature08121_S1.html

[8] M. Hofheinz, H. Wang, M. Ansmann, R. C. Bialczak, E. Lucero, M. Neeley, A. D. O'Connell, D. Sank, J. Wenner, J. M. Martinis, A. N. Cleland, Synthesizing arbitrary quantum states in a superconducting resonator, Nature 459 (7246) (2009) 546–549.
URL http://dx.doi.org/10.1038/nature08005http://www.nature.com/nature/journal/v459/n7246/suppinfo/nature08005_S1.html

[9] A. A. Abdumalikov Jr., O. Astafiev, A. M. Zagoskin, Y. A. Pashkin, Y. Nakamura, J. S. Tsai, Electromagnetically Induced Transparency on a Single Artificial Atom, Physical Review Letters 104 (19) (2010) 193601.
URL http://link.aps.org/doi/10.1103/PhysRevLett.104.193601

[10] O. V. Astafiev, A. A. Abdumalikov Jr., A. M. Zagoskin, Y. A. Pashkin, Y. Nakamura, J. S. Tsai, Ultimate On-Chip Quantum Amplifier, Physical Review Letters 104 (18) (2010) 183603.
URL http://link.aps.org/doi/10.1103/PhysRevLett.104.183603

[11] A. A. Houck, H. E. Tureci, J. Koch, On-chip quantum simulation with superconducting circuits, Nat Phys 8 (4) (2012) 292–299.
URL http://dx.doi.org/10.1038/nphys2251

[12] R. Feynman, Simulating physics with computers, International Journal of Theoretical Physics 21 (6) (1982) 467–488.
URL http://dx.doi.org/10.1007/BF02650179

[13] P. W. Shor, Algorithms for quantum computation: discrete logarithms and factoring (1994).

[14] L. K. Grover, A fast quantum mechanical algorithm for database search, in: Proceedings of the twenty-eighth annual ACM symposium on Theory of computing, STOC '96, ACM, New York, NY, USA, 1996, pp. 212–219.
URL http://doi.acm.org/10.1145/237814.237866

[15] M. A. Nielsen, I. L. Chuang, Quantum Computation and Quantum Information, Cambridge University Press, 2000.

[16] I.-C. Hoi, C. M. Wilson, G. Johansson, T. Palomaki, B. Peropadre, P. Delsing, Demonstration of a Single-Photon Router in the Microwave Regime, Physical Review Letters 107 (7) (2011) 73601.
URL http://link.aps.org/doi/10.1103/PhysRevLett.107.073601

[17] V. Bouchiat, D. Vion, P. Joyez, D. Esteve, M. H. Devoret, Quantum coherence with a single Cooper pair, Physica Scripta 1998 (T76) (1998) 165.
URL http://stacks.iop.org/1402-4896/1998/i=T76/a=024

[18] Y. Nakamura, Y. A. Pashkin, J. S. Tsai, Coherent control of macroscopic quantum states in a single-Cooper-pair box, Nature 398 (6730) (1999) 786–788.
URL http://dx.doi.org/10.1038/19718

[19] J. R. Friedman, V. Patel, W. Chen, S. K. Tolpygo, J. E. Lukens, Quantum superposition of distinct macroscopic states, Nature 406 (6791) (2000) 43–46.
URL http://dx.doi.org/10.1038/35017505

[20] C. H. van der Wal, A. C. J. ter Haar, F. K. Wilhelm, R. N. Schouten, C. J. P. M. Harmans, T. P. Orlando, S. Lloyd, J. E. Mooij, Quantum Superposition

of Macroscopic Persistent-Current States , Science 290 (5492) (2000) 773–777.
URL http://www.sciencemag.org/content/290/5492/773.abstract

[21] J. M. Martinis, S. Nam, J. Aumentado, C. Urbina, Rabi Oscillations in a Large Josephson-Junction Qubit, Physical Review Letters 89 (11) (2002) 117901.
URL http://link.aps.org/doi/10.1103/PhysRevLett.89.117901

[22] J. Koch, T. M. Yu, J. Gambetta, A. A. Houck, D. I. Schuster, J. Majer, A. Blais, M. H. Devoret, S. M. Girvin, R. J. Schoelkopf, Charge-insensitive qubit design derived from the Cooper pair box, Physical Review A 76 (4) (2007) 42319.
URL http://link.aps.org/doi/10.1103/PhysRevA.76.042319

[23] A. Cottet, Implementation of a quantum bit in a superconducting circuit, Ph.D. thesis, Universit{é} Paris VI (2002).

[24] A. Houck, J. Koch, M. Devoret, S. Girvin, R. Schoelkopf, Life after charge noise: recent results with transmon qubits, Quantum Information Processing 8 (2) (2009) 105–115.
URL http://dx.doi.org/10.1007/s11128-009-0100-6

[25] A. Fedorov, L. Steffen, M. Baur, A. Wallraff, Implementation of a Toffoli Gate with Superconducting Circuits, Nature 481 (7380) (2011) 4.
URL http://arxiv.org/abs/1108.3966

[26] L. DiCarlo, M. D. Reed, L. Sun, B. R. Johnson, J. M. Chow, J. M. Gambetta, L. Frunzio, S. M. Girvin, M. H. Devoret, R. J. Schoelkopf, Preparation and measurement of three-qubit entanglement in a superconducting circuit, Nature 467 (7315) (2010) 574–578.
URL http://dx.doi.org/10.1038/nature09416http://www.nature.com/nature/journal/v467/n7315/abs/nature09416.html#supplementary-information

[27] V. B. Braginsky, F. Y. Khalili, Quantum nondemolition measurements: the

route from toys to tools, Reviews of Modern Physics 68 (1) (1996) 1–11.
URL http://link.aps.org/doi/10.1103/RevModPhys.68.1

[28] M. Brune, S. Haroche, V. Lefevre, J. M. Raimond, N. Zagury, Quantum non-demolition measurement of small photon numbers by Rydberg-atom phase-sensitive detection, Physical Review Letters 65 (8) (1990) 976–979.
URL http://link.aps.org/doi/10.1103/PhysRevLett.65.976

[29] P. Grangier, J. A. Levenson, J.-P. Poizat, Quantum non-demolition measurements in optics, Nature 396 (6711) (1998) 537–542.
URL http://dx.doi.org/10.1038/25059

[30] A. La Porta, R. E. Slusher, B. Yurke, Back-Action Evading Measurements of an Optical Field Using Parametric Down Conversion, Physical Review Letters 62 (1) (1989) 28–31.
URL http://link.aps.org/doi/10.1103/PhysRevLett.62.28

[31] M. D. Levenson, R. M. Shelby, M. Reid, D. F. Walls, Quantum Nondemolition Detection of Optical Quadrature Amplitudes, Physical Review Letters 57 (20) (1986) 2473–2476.
URL http://link.aps.org/doi/10.1103/PhysRevLett.57.2473

[32] G. Nogues, A. Rauschenbeutel, S. Osnaghi, M. Brune, J. M. Raimond, S. Haroche, Seeing a single photon without destroying it, Nature 400 (6741) (1999) 239–242.
URL http://dx.doi.org/10.1038/22275

[33] B. Peropadre, G. Johansson, Scattering of a single photon on a single artificial atom, In preparation.

[34] C. W. Gardiner, P. Zoller, Quantum Noise, Springer, 2004.

[35] R. Loudon, The Quantum Theory of Light, Oxford University Press, 2000.

[36] A. F. Kockum, Transmons in transmission line with (S,L,H), Personal Communication.

[37] N. Matsuda, R. Shimizu, Y. Mitsumori, H. Kosaka, K. Edamatsu, Observation of optical-fibre Kerr nonlinearity at the single-photon level, Science And Technology 3 (February) (2009) 95–98.
URL `http://www.nature.com/doifinder/10.1038/nphoton.2008.292`

[38] N. Matsuda, Y. Mitsumori, H. Kosaka, K. Edamatsu, R. Shimizu, Lossless all-optical phase gate using a polarization-division Sagnac interferometer applicable to a waveguide-type Kerr medium, Applied Physics Letters 91 (17) (2007) 171119.
URL `http://link.aip.org/link/APPLAB/v91/i17/p171119/s1&Agg=doi`